Journal of Applied Physics

Nanofabrication by thermal plasma jets: From nanoparticles to low-dimensional nanomaterials

Cite as: J. Appl. Phys. **125**, 070901 (2019); https://doi.org/10.1063/1.5060977
Submitted: 21 September 2018 . Accepted: 20 January 2019 . Published Online: 19 February 2019

K. S. Kim, and T. H. Kim

COLLECTIONS

This paper was selected as Featured

View Online Export Citation CrossMark

ARTICLES YOU MAY BE INTERESTED IN

Perspective: Nanoscopy of charge kinetics via terahertz fluctuation
Journal of Applied Physics **125**, 010901 (2019); https://doi.org/10.1063/1.5079534

Phonon properties and thermal conductivity from first principles, lattice dynamics, and the Boltzmann transport equation
Journal of Applied Physics **125**, 011101 (2019); https://doi.org/10.1063/1.5064602

Tutorial: Brain-inspired computing using phase-change memory devices
Journal of Applied Physics **124**, 111101 (2018); https://doi.org/10.1063/1.5042413

Lock-in Amplifiers
Find out more today

Zurich Instruments

Journal of Applied Physics PERSPECTIVE scitation.org/journal/jap

Nanofabrication by thermal plasma jets: From nanoparticles to low-dimensional nanomaterials

Cite as: J. Appl. Phys. **125**, 070901 (2019); doi: 10.1063/1.5060977
Submitted: 21 September 2018 · Accepted: 20 January 2019 ·
Published Online: 19 February 2019

View Online Export Citation CrossMark

K. S. Kim[1,2] and T. H. Kim[3]

AFFILIATIONS

[1]Security and Disruptive Technologies Research Centre, Emerging Technologies Division, National Research Council Canada, Ottawa, Ontario K1A 0R6, Canada
[2]Department of Mechanical and Industrial Engineering, University of Toronto, 5 King's College Road, Toronto, Ontario M5S 3G8, Canada
[3]Institute for Nuclear Science and Technology, Jeju National University, Jeju 63243, Republic of Korea

ABSTRACT

Current fabrication of nanomaterials is facing the following two challenges: high selectivity toward specific chemical compositions or morphologies and their scalable production. This usually requires new extreme fabrication conditions beyond the conventional approaches. Thermal plasma jets are flows of partially ionized gases where gas and electron temperatures reach their equilibrium state around 10 000 K, and thus provide high fluxes of energy and chemically active species including electrons and ions with their strong spatial gradients. Such extreme environments can trigger reactions that are not thermodynamically favorable or require high activation barriers, leading to the production of materials with exotic chemical compositions or structures. Since their first operation in 1960, thermal plasma jets were soon recognized as a unique and effective medium for material transformation such as melting, vaporization, and pyrolysis and recently have also found their important applications in nanomaterial fabrication. In this Perspective, we briefly review the latest progress in the thermal plasma jet-assisted fabrication of nanomaterials from nanoparticles to low-dimensional nanostructures. A special focus is made on the advantages of the thermal plasma jet technology in nanostructure fabrication, discussing plasma properties responsible for the nanomaterial growth with high throughput, high purity, anisotropy, desired compositions, or narrow size distributions. This Perspective closes with an outlook of challenges and opportunities for further advancement in this emerging field.

https://doi.org/10.1063/1.5060977

I. INTRODUCTION

High-intensity arc discharge generated by either direct or radio-frequency (RF) current can be further stabilized by gas flow in a confinement channel. The gas is rapidly heated by the arc column and expands after the confinement nozzle which leads to the formation of a stream of hot gas known as a thermal plasma jet. Its temperature can reach up to 20 000 K and velocities ranging from several m/s to supersonic range can be obtained depending on the nozzle design.[1] Since their initial development in the mid-1960s, thermal plasma jets have been extensively used as heat sources in various materials' transformation processes (e.g., melting, vaporization, and pyrolysis) taking advantage of their unique features of high temperatures (1000–10 000 K) and high heat contents (a few MJ/kg) and have represented an attractive and versatile opportunity in material processing applications such as metal refinement, spray coating of refractory materials, cutting, welding, waste treatments, and so on.[2–5]

In addition to the material transformation, since mid-1970s, thermal plasma jets were rapidly recognized to facilitate chemical or physical growths of pure or composite (e.g., oxides, carbides, nitrides, borides) particles with submicron sizes.[6–9] Such nano-size particles, whose sizes range from a few tens of nanometers to a few hundreds of nanometers, have many potential applications owing to their high surface-to-volume ratios. In the past 40 years, thermal plasma jets have been proven to be very efficient in the synthesis of various nanoparticles utilizing any kind of precursor in different physical forms or chemical compositions.[10–13] The presence of abundant radical species as well as electrons and ions not only facilitates fast reactions but also opens up new chemical pathways for efficient nucleation and growth of nanoparticles

with specific compositions and morphologies. Thermal plasma jets often provide extremely high cooling rates of 10^5–10^6 K/s due to the plasma jet expansion or additional quenching gas injection which can prevent particles from continuously growing to larger particles. The rapid heating and subsequent cooling of materials by thermal plasma jets is also highly favorable for size reduction via partial vaporization of micro-sized particles or thermal-shock driven exfoliation of layered bulk materials. Lastly, the entire process is truly continuous and scalable compared to other similar high-temperature methods such as laser vaporizations where feedstock is supplied as consumable targets. In a thermal plasma process, the feedstock is injected into a plasma jet and the reaction products embedded in the gas stream are separated continuously through filtration. To date, syntheses of various kinds of nanoparticles, including oxides, carbides, nitrides, borides, metals, and composite materials, have been successfully demonstrated by thermal plasma jets with high throughputs [Fig. 1(a)]. In this Perspective, we will review recent progress with representative examples.

With the advent of the nano era expedited by the discoveries of fullerenes and carbon nanotubes,[14–16] such potential has been further extended to the fabrication of various nanomaterials with low-dimensionalities (zero-, one-, or two-dimensions). Unlike conventional three-dimensional (3D) materials, such geometrical constraints limit the motion of electrons to two or fewer dimensions. Such confinement effects at the

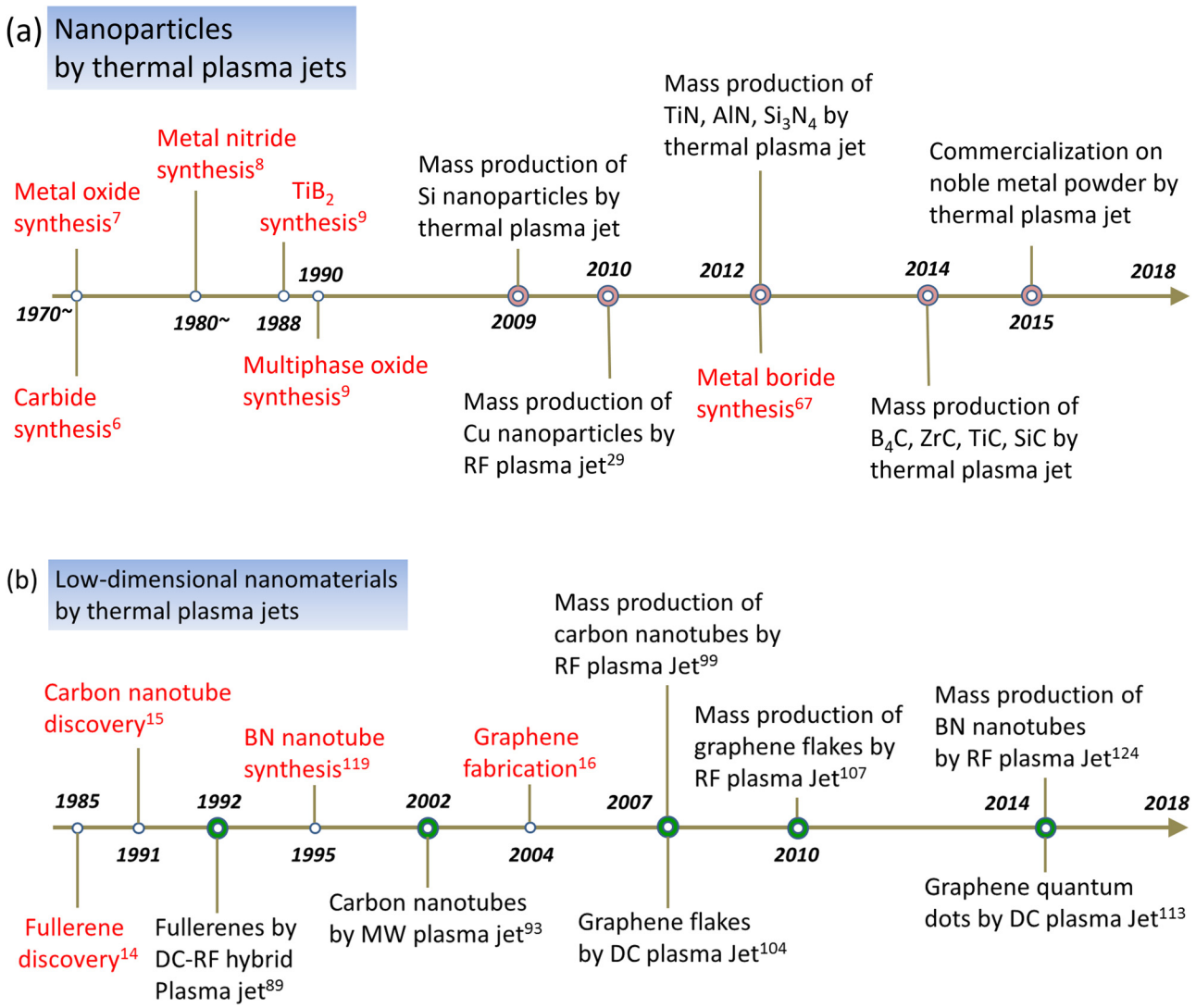

FIG. 1. Timeline of the major breakthroughs in the thermal plasma synthesis of (a) nanoparticles and (b) low-dimensional nanomaterials.

nanoscale usually impart intriguing properties to materials exhibiting unusual electronic or optical behaviors that have never been observed before with conventional 3D bulk materials. The molecular backbones of such low-dimensional nanomaterials are also mechanically robust making them appealing for many lightweight structural reinforcement applications in defense and security, aerospace, and automotive sectors. Therefore, there have been strong scientific and industrial interests to these materials including quantum dots, nanotubes, and atomically thin layers of various layered materials. However, their low production volumes combined with uncontrolled structural properties (e.g., diameter, chirality, grain size, and wall numbers) still remain a challenge in the exploitation of their real-world applications. Although thermal plasma jets have been widely used in nanoparticle fabrication, their fabrication of low-dimensional nanostructures is a relatively new interest in plasma science and technology. Despite this, there have been notable advancements of this field achieved by the thermal plasma jet technology [Fig. 1(b)]. This Perspective reviews those progresses as well.

In both cases, challenges and opportunities exist in further optimization of the current processes or in the design of new synthesis methods using thermal plasma jets. Unravelling the roles of plasma jets is of critical importance in such developments, while the underlying physics behind nanomaterial growth under various plasma conditions has not been fully understood due to high temperatures with steep gradients, complicated interactions between plasma and materials, turbulences, and so on. Recently, there have been significant attempts to answer the above open question by revealing plasma properties responsible for nanomaterial growth with high throughput, high purity, anisotropy, desired compositions, or narrow size distributions, based on computational modeling and plasma diagnostics. An outlook is given with a review of the latest advancement in this regard, followed by a brief discussion of synthesis of new revolutionary materials where unique advantages of thermal plasma jets may exist.

II. THERMAL PLASMA JETS

A. Generation and characteristics

Thermal plasma jets are generated by electrical arc heaters, so-called thermal plasma torches. Thermal plasma torch technology is matured and various types of torches are commercially available with a wide range of power levels (kW to MW). As an efficient and environmentally clean heat source, many thermal plasma torches have already found their unique applications in the materials industry. For a thorough review of this technology, there are excellent review articles available in the literature.[2–5]

In nanomaterial fabrication, there have been two types of thermal plasma torches widely used: direct current (DC) plasma torches and radio-frequency (RF) plasma torches. A schematic diagram illustrating their key features is shown in Fig. 2. A DC torch typically consists of a cathode and an anode nozzle and can be broadly classified into the rod- and hollow-type electrode according to the shape of electrodes or non-transferred and transferred-type depending on the arrangement of electrodes. A rod-type cathode is typically made of 2% thoriated tungsten with a conical shape and electrons are supplied by thermionic emission (i.e., hot cathode). With a tungsten cathode, oxygen-containing gases should be avoided because the oxide layer formed is volatile at relatively low temperatures (~1700 °C) causing severe erosion.[17] However, other refractory materials such as hafnium or zirconium, whose oxides have higher melting or boiling temperatures, can be used with the oxygen-containing gas.[17,18] A hollow cathode is commonly made of oxygen-free high purity copper and cooled by water; thus, electrons are supplied by positive ion bombardment rather than thermionic emission (i.e., cold

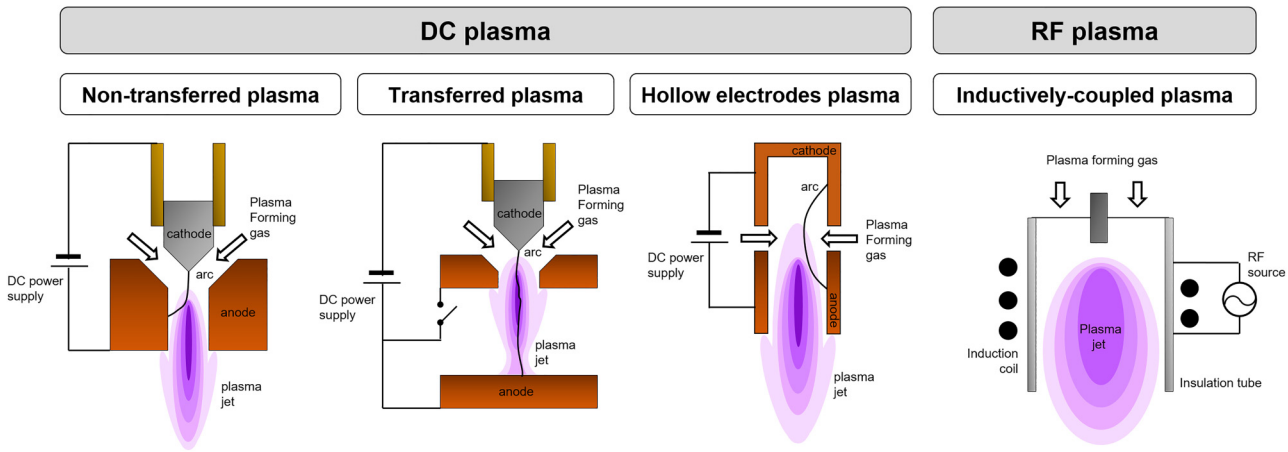

FIG. 2. Illustration of various thermal plasma torches used in nanomaterial fabrication.

cathode). Any kinds of gases including air or steam can be used.[19] A transferred-type torch uses workpiece as an electrode; thus, higher thermal efficiency is obtained compared to a non-transferred type torch. In a DC plasma torch, the electric arc is initially generated by applying a high-voltage (a few kV) between the cathode and anode electrodes (or pilot electrode for the transferred-type torch), and gases are flown around the arc column for heating via conductive, convective, and radiative heat exchanges. A nozzle is used at the end of the torch to expand the heated gas and form a plasma jet. The jet conditions (e.g., temperature, velocity, and species fields) are largely dictated by the nozzle design and thus can be customized for an efficient synthesis of nanomaterials. A typical non-transferred DC torch with a rod-type cathode produces a plasma jet with temperature in the range of 8000–16 000 K at the torch exit and velocity ranging from a few hundreds of m/s to several thousands of m/s depending on the nozzle geometry.[20–22] By using a convergent-divergent nozzle (e.g., Laval nozzle), the jet velocity can reach a supersonic velocity by converting the heat energy into the kinetic energy and readily realize non-equilibrium chemistry which is not favorable thermodynamically. There are a couple of advantages of DC plasma torches in nanofabrication. The relatively small diameter of the DC plasma torch constricts the plasma jet produced increasing the temperature and velocity maximums at the torch axis. An overall efficiency above 70% is also much higher than that of the RF plasma torch. Compared to RF plasma jets, DC plasma jets are mostly turbulent which usually enhances mixing of the precursors injected;[23] however, electrode erosion by the arc root attachments may cause unwanted contamination of the product or inefficiency of the process due to frequent electrode replacements.

An RF plasma torch is typically composed of a confinement tube and an electromagnetic coil.[24] For better control of the plasma jet, a nozzle can be attached to the end of the torch exit. The sustainment of plasma in an RF plasma torch is accomplished by the induction heating mechanism; an oscillating current in the coil generates an alternating magnetic field inside the confinement tube where an electrically conducting medium (i.e., plasma) is present. Under the alternating magnetic field, eddy currents are generated in the medium and dissipate heat via the Joule heating process. This energy is enough for continuous ionization of the injected gas, thus sustaining the plasma. The induction plasma torch has several advantages over the DC plasma torch in materials processing.[25] Thanks to its electrodeless design, it is free from contamination, thus better suited for high-purity material processing than the DC torch. This also allows injection of almost any kind of feedstock or reactant into the plasma core region, achieving a better heat and momentum transfer between plasma and materials. The RF plasma torch usually provides a larger volume of hot zone (5000–10 000 K) with a moderate velocity ranging from several tens of m/s to hundreds of m/s. This increases the residence time of the feedstock in the plasma region, significantly enhancing the growth of materials. However, its relatively low temperature maximum and power efficiency (<70%) still remain challenges to address. Other than DC or RF plasma torches, microwave (MW) plasma torches have also been widely used in the fabrication of nanomaterials.[26–28] The MW plasma is sustained by the electromagnetic surface wave launched from a microwave source (e.g., a magnetron in a microwave oven with a typical frequency of 2.45 GHz) and stabilized by the swirl injection of gases. MW plasma torches are also electrodeless but provide a higher coupling efficiency compared to RF plasma torches.

B. Principle of nanofabrication by thermal plasma jets

In the thermal plasma jet process, nanomaterials are fabricated by either bottom-up or top-down approach (Fig. 3). In the bottom-up approach [Fig. 3(a)], feedstock or precursor materials are injected into a hot plasma plume (>5000 K) and vaporize immediately. Then, the resulting vapors undergo a rapid quench (~10^6 K/s) through plasma jet expansion. Such supersaturation of vapors provides a strong driving force for the nucleation of nanoparticles via homogeneous nucleation. Once nanoparticles are formed, they continue to grow through surface reactions, such as co-condensation and coagulation. In order to limit the size to submicron, additional quenching gases such as argon or helium are commonly introduced downstream. The processed materials are separated continuously from the gas stream by *in situ* filtration. Prior to the filtration, a cyclone separator is often employed to remove larger or untreated particulates from the reaction products. Finally, the collected materials are treated in a glovebox for their safe handling or passivation if needed, especially for highly reactive metal nanoparticles.

The top-down approach has also been employed to produce nanomaterials using thermal plasma jets [Fig. 3(b)]. Some natural bulk materials are composed of many atomically-thin layers held by the relatively weak van der Waals (vdW) force. Typical examples are graphite, hexagonal boron nitride (hBN), black phosphorus, and transition metal dichalcogenides (TMDCs). The spaces between the layers of those materials can easily accommodate small ions, atoms, or molecules (i.e., intercalation) via proper treatments (e.g., acid treatment). This results in the expansion of the lattice space which greatly facilitates the cleavage of layered materials upon rapid heating. The intercalants expand dramatically due to the heat causing layered bulk materials to exfoliate into smaller layers or nano-size platelets. Thermal plasma jets are capable of rapid heating of materials and thus have also been studied for effective exfoliation of layered materials.

III. SYNTHESIS OF NANOPARTICLES

In the thermal plasma jet process, nanoparticles are produced from various gas-phase chemical reactions as bottom-up approach. Figure 4 presents Gibbs free energies (ΔG) of oxidation, carbonization, nitridation, and boridation reactions representatively calculated for a wide range of temperature from 500 to 7000 K (HSC Chemistry 9, Outotec Technologies, Finland). Most of the oxidation reactions are spontaneous with high negative ΔG for the entire temperature range considered [Fig. 4(a)]. Therefore, it is estimated

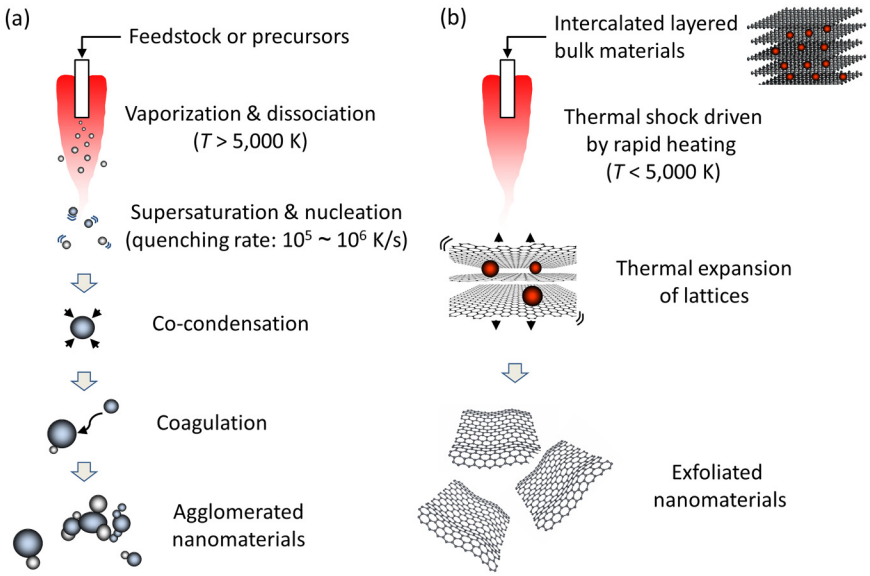

FIG. 3. Principle of nanofabrication by thermal plasma jets. (a) Bottom-up and (b) top-down approaches.

that the oxide material is synthesized comfortably with reactive species in the thermal plasma process. However, some carbonization, nitridation, and boridation reactions are expected to occur in the specific temperature range with appearance of positive ΔG values [see Figs. 4(b)–4(d)], suggesting that control of temperature to a proper range would be critical to maximize those reactions. The thermal flow environment should be controlled properly according to the operating or design variables in the plasma process. A detailed discussion of Gibbs free energy of each chemical reaction will be given in Secs. III B, III C, III D, and III E.

A. Pure metal nanoparticles

From the late 1990s, many kinds of metal nanoparticles were prepared by the thermal plasma jet technology including aluminum, gold, nickel, copper, silver, tungsten, iron, and so on.[29–32] Unlike the combustion process, thermal plasmas can be readily generated in an oxygen-free environment; thus, preparation of metal nanoparticles from their precursors is relatively simple. In the thermal plasma process, metal lumps or micron-size metal powders are commonly used as precursors.

In the case of metal lumps, it can be employed as a consumable electrode of a transferred-type DC thermal plasma torch and vaporized directly by contact with a high enthalpy arc. The metal vapors formed condense immediately upon escaping the hot arc zone and turn into nano-size particles. However, effective vaporization of the starting material is limited because the thermal conductivity of the metal melt formed rapidly decreases due to the excessive heat loss to the crucible. The optimum design of the crucible is a matter of vital importance to maintaining good thermal conductivity of the metal melt. Since 2015, nonetheless, the noble metal nanopowders prepared by this method have been commercialized to produce sputtering targets for semiconductor industries (Heesung Metal Ltd, Republic of Korea).

For the micron-size metal powder precursors, both non-transferred-type DC and RF thermal plasma jets can be applied to reduce the particle size through an in-flight vaporization-condensation process. As an example, bulk silicon has a theoretical discharge capacity of 4200 mAh/g which is 10 times larger than that of graphite, thus pushes the limit of current lithium ion battery technology. However, its large volume change of 400% during operation has been a critical issue attracting more attention toward its nanomaterials as they can minimize the volume expansion. Conversions of micron-sized silicon powders (~40 μm) to their spherical nanoparticles (<100 nm) were reported using both DC (10–13 kW, 101 kPa, Ar plasma) and RF (4 MHz, 25 kW, 65 kPa, Ar/H_2 plasma) thermal plasma jets.[33,34] Lee *et al.*[33] revealed that the quality of silicon nanoparticles prepared by an RF thermal plasma can be improved by using a counterflow quenching gas. The particle size became smaller (~30 nm) with a narrow size distribution ranging from 10 to 60 nm. The counterflow usually generates recirculation eddies that trap injected or newly formed particulates increasing their residence time in the high temperature region. It is able to improve the vaporization efficiency of the feedstock minimizing the contamination by feedstock residues, while it can also increase the particle size produced through coagulation. Thus, optimum design of the flow pattern is of critical importance to the efficient synthesis of nanoparticles and a numerical simulation work was reported by Colombo *et al.*[35]

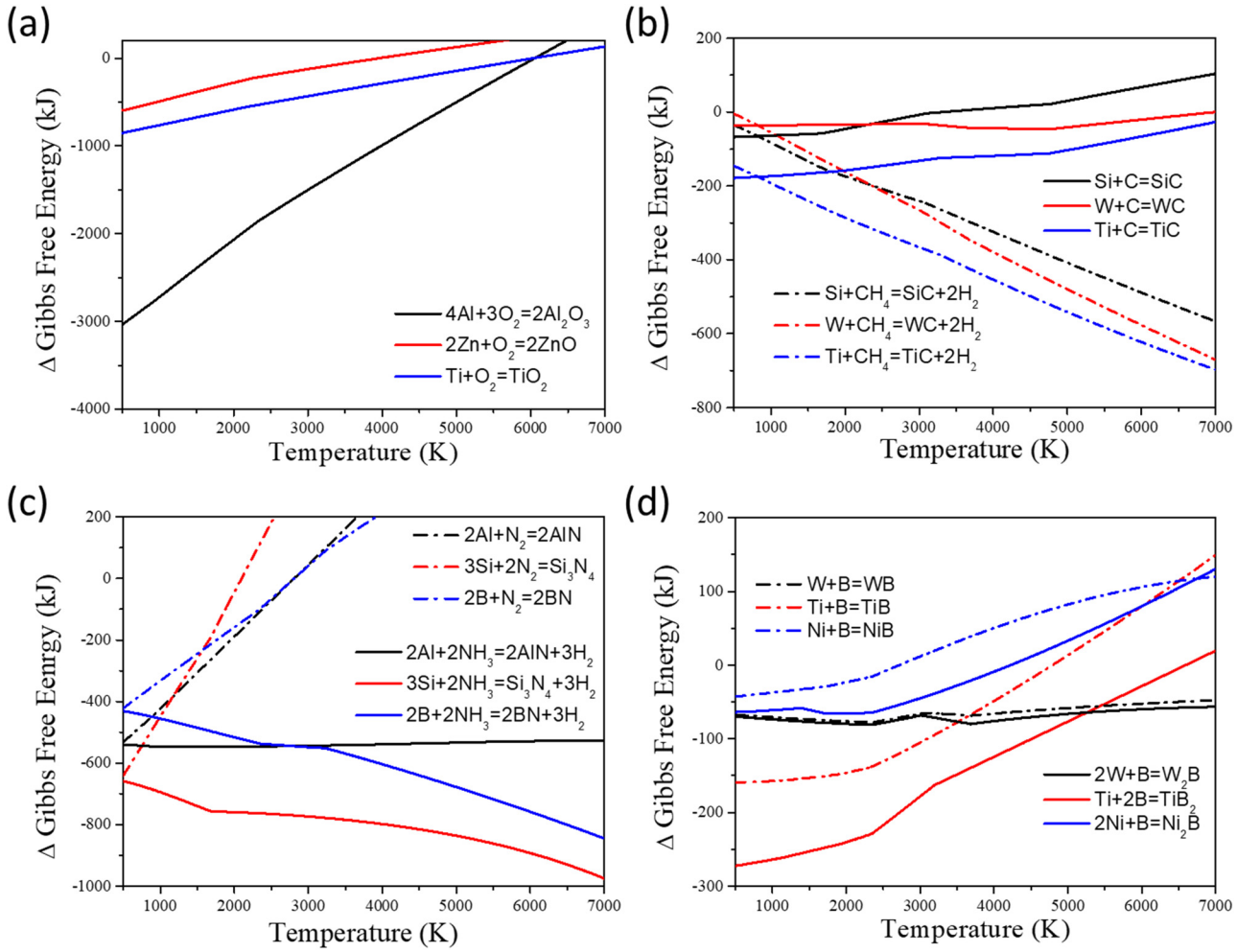

FIG. 4. Gibbs free energies of (a) oxidation, (b) carbonization, (c) nitridation, and (d) boridation reactions by thermodynamic equilibrium calculation.

Spherical metal nanoparticles have a great impact on the additive manufacturing industry by providing high packing density and high flowability. Metal particles molten by a plasma jet form spherical droplets to reduce the surface tension and also continue to vaporize reducing their size. Upon rapid quenching, they solidify to spherical nanoparticles. Various spherical metal nanopowders (Al, Cu, Ag, Ni, Fe, Co, Mo, Ta, Si, W, Re, B; mean size: 15–200 nm) have been produced by an DC and RF thermal plasma and Cu and Si nanoparticles are commercially available from TEKNA in Canada and Hefei Kaier Nano Energy Technology in China.[36]

B. Metal oxide nanoparticles

Metal oxide nanoparticles exhibit excellent resistance toward high heat fluxes and corrosive chemicals playing an important role for various industrial applications in paint and coating, automobile, construction, aerospace, medicine, and packaging industries. The metal oxide nanoparticle market is expected to grow at a CAGR (compound annual growth rate) of 10.5% during 2016–2022. Metal oxides are typically synthesized through oxidation reactions that are mostly exothermic; thus, high temperature environments may not be favorable for the formation of oxides (Le Châtelier's principle). This is also supported by the ΔG calculations shown in Fig. 4(a), where ΔG continues to increase with temperature. For this reason, the main interest in this field has been their mass production with controlled phase structures and sizes rather than achieving extremely high temperature conditions.

Titanium oxide (TiO_2) nanoparticles are commonly synthesized as a mixture of several phases, such as anatase and rutile phases. Since they have different properties and applications, synthesis of TiO_2 with controlled structures was extensively studied using thermal plasma jets.[37–39] In an RF

thermal plasma process (2 MHz, 25–40 kW, 53–80 kPa, Ar/O, Ar/He/O_2, Ar/H_2/CO_2 plasmas), it is found that the ratio of anatase and rutile phases can be controlled (20–75 wt. %) by the oxygen content in the plasma gas and the thermal history of TiO_2 particles nucleated. This ratio increased with oxygen concentration due to the oxygen-deficient nature of the rutile phase, while a rapid cooling promoted formation of the rutile phase reducing the reaction time of TiO_2 particles with oxygen. To study the effects of cooling rates, several modes of quenching gas injection (radial, counter, and swirl injections) have been studied with different cooling gases (Ar or He).[40]

In the 2000s, various kinds of doped metal oxide nanoparticles have been studied by using thermal plasma with the drastic growth of renewable energy sectors. For photocatalytic applications, TiO_2 was mostly studied with various dopants of carbon,[41] aluminum,[42,43] and copper.[40] By doping TiO_2 nanoparticles, their photocatalytic activity in the ultraviolet region was extended to the visible region. The degree of doping was controllable by adjusting the concentration of dopants in the precursors.

C. Metal carbide nanoparticles

Metal carbide materials have been considered high-value products with exceptional hardness and thermal/chemical stability. Tantalum (TaC) and hafnium carbides (HfC) are ultra-high temperature ceramics with very high melting points of about 4000 °C. Spherical tungsten carbide (WC) particles are used as hardfacing surface coatings to withstand high thermal/mechanical stress, as well as electric catalysts with high electrocatalytic performances. As shown in Fig. 4(b), some carbonizing reactions of metals (e.g., reaction with methane) are more thermodynamically favorable at high temperatures with decreasing ΔG; thus, thermal plasmas are highly suited for the synthesis of various carbide nanoparticles.

Silicon carbide nanoparticles less than 80 nm were synthesized from a mixture of silicon tetrachloride ($SiCl_4$) and methane gas using a DC thermal plasma jet (8–12 kW, 101 kPa, Ar/H_2 plasma).[44] It was found that the addition of hydrogen increased the conversion rate because hydrogen enhances the decomposition and reduction of silicon chloride compounds ($SiCl_x$). Titanium carbide and tantalum carbide nanoparticles were synthesized by DC and RF thermal plasma systems, respectively.[45,46] Ishigaki *et al.*[46] employed tantalum ethoxide [$Ta(OC_2H_5)_5$] as a liquid precursor to supply both metal and carbon sources simultaneously to an RF thermal plasma (2 MHz, 40 kW, 53–100 kPa, Ar/H_2/CO_2 plasma). It was noted that an increasing molar ratio of H_2 to $Ta(OC_2H_5)_5$ improved the TaC yield to 97.4 wt. % owing to selective etching of solid carbon impurities by hydrogen atoms. However, excessive hydrogen promoted decomposition of TaC to the Ta phase. By employing a low pressure of 53 kPa and additional He quenching gas, the average particle size was decreased to 8 nm and its distribution became narrow due to the rapid cooling of the reaction stream.

The hardness of WC particles larger than 1 μm increases linearly with their size, while it increases exponentially for particles smaller than 100 nm. Moreover, their deflective strength also improves in the nanoscale; thus, preparation of WC nanoparticle has been of particular interest. Since the first demonstration by Ronsheim *et al.* in 1981,[47] numerous thermal plasma syntheses of WC were reported to date via particle-particle reaction, particle-gas reaction, and gas-gas reactions, the important limitation being low purity.[48–51] Unlike other metal carbides prepared by thermal plasma, most WC products were composed of a mixture of several phases of tungsten compound such as stable WC and metastable W_2C or WC_{1-x} with unreacted tungsten powders. Despite considerable efforts to optimize the condition of a DC plasma process (11–32 kW, 101 kPa, Ar plasma, WCl_6/H_2/CH_4 precursors), formation of metastable WC_{1-x} phase was always predominant.[51] The produced W_2C and WC_{1-x} nanoparticles can be carburized completely to form WC phase by post hydrogen treatment at 900 °C for 5 h; however, the size of the final particles increased from 20 nm to 100 nm during the heat treatment.[51] The one-step, phase controlled synthesis of WC nanoparticles by the thermal plasma still remains a challenge.

D. Metal nitride nanoparticles

Metal nitride nanomaterials have various industrial applications as refractory ceramics particularly for catalysts, semiconductor devices for optoelectronics, and wear-resistant coatings. Similar to the carbonizing reactions above, some nitriding reaction of metals (e.g., reaction with ammonia) are more thermodynamically favorable at high temperatures with decreasing ΔG [Fig. 4(c)]; thus, thermal plasmas are also highly effective for the synthesis of nitride nanoparticles. Many metal nitride nanoparticles have been synthesized using DC, RF, and microwave thermal plasmas; aluminum nitride (AlN),[52–54] silicon nitride (Si_3N_4),[55–58] titanium nitride (TiN),[58–60] magnesium nitride (Mg_3N_2),[61] boron nitride (BN),[62–64] gallium nitride (GaN),[65] and so on. In those studies, solid or gas phase precursors were used as the metal sources, whereas nitrogen or ammonia gases were commonly used as the nitridation agents.

In the previous thermal plasma processes, while most metal nitride nanoparticles were synthesized with high crystallinity, synthesis of crystalline silicon nitride (α-Si_3N_4) nanoparticles has been very challenging. Most reaction products were either heavily contaminated by silicon nanoparticle by-products (2.45 GHz microwave plasma, 101 kPa, 1 kW, Ar/N_2/H_2 plasma, $SiCl_4$ precursor) or less crystallized (DC, 10–11 kW, Ar plasma, $SiCl_4$/NH_3/H_2 precursors, 15–75 kPa). This is because exposure to temperatures above 1850 °C will decompose Si_3N_4 produced into Si and nitrogen, while low temperatures are not favorable for the *in situ* annealing of Si_3N_4 produced to form α-Si_3N_4 phase. The crystal phase (α-Si_3N_4) was obtained either by annealing the produced amorphous Si_3N_4 at 1500 °C under the nitrogen atmosphere or processing micro-sized α-Si_3N_4 powders via in-flight size reduction in an RF thermal plasma jet (4 MHz, 10 kW, 0.49–0.98 kPa, Ar plasma, $SiCl_4$/NH_3 precursors).[57] Gallium nitride nanoparticles also have a similar issue.[65]

The boron nitride (BN) is a polymorphic material with two common crystalline structures of hexagonal (hBN) and cubic (cBN) forms. The hexagonal form is the most stable crystal structure in ambient conditions, while the cubic form is stable only in extreme conditions such as high pressure and high temperature environments. The cubic phase possesses exceptional hardness, thermal conductivity, and electrical resistivity that are almost comparable to those of diamond; thus, mass production of BN nanomaterials has been of particular interest but is both difficult and expensive. Both hBN and cBN nanoparticles were synthesized by DC thermal plasma torches depending on the precursors employed.[62,63] Cubic-BN nanoparticles less than 150 nm were synthesized by a DC plasma jet (13 kW, 101 kPa, Ar/N_2 plasma) using a mixture of boron oxide (B_2O_3) and melamine ($C_3H_6N_6$) as a precursor. Melamine served as a reducing agent as well as a source of various exothermic gases, such as CO, CO_2, H_2, and N_2, which release additional heat upon capturing oxygen or recombination. Although the growth mechanism of c-BN nanoparticles in this plasma process is still not fully understood, it was speculated that the extreme high temperature of the thermal plasma jet and additional heat from exothermic reactions play an important role in the cBN formation.

E. Metal boride nanoparticles

The successful preparation of sub-micron titanium boride (TiB_2) powders by an arc heater promoted studies of synthesis of various metal boride nanoparticles by the thermal plasma in the 2010s. The metal borides are classified as either boron-rich (e.g., most boron-rich boride: YB_{66}) or metal-rich borides (e.g., most metal-rich boride: $Nd_2Fe_{12}B$). Owing to their strong covalent boron-boron and metal-boron bonds, metal borides exhibit excellent thermal and mechanical properties such as high melting points over 3000 K, wear resistance, and chemical inertness.[66] In addition, borides have large neutron absorption cross sections due to the presence of elemental boron, thus highly attractive for the fabrication of mechanical parts under extreme conditions (e.g., high temperature or radiative environments). As shown in Fig. 4(d), boridation reaction is most thermodynamically challenging with relatively high values of ΔG compared with other reactions. In addition, to avoid contamination, pure boron and metal powders are commonly employed as feedstock whose vaporization temperatures are well above a few thousand degree Celsius. This makes thermal plasmas better suited for metal boride preparations; however, it should be noted that some boridation reactions are not thermodynamically favorable at temperatures above 4000 K (e.g., TiB_2), as shown in Fig. 4(d). Controlling the processing temperature to a proper range is critical to produce metal borides with a high purity level.

Various metal boride nanoparticles, including aluminum boride (AlB_{12}),[66] yttrium boride (YB_{66}),[66] titanium boride (TiB and TiB_2),[67,68] iron boride (FeB and Fe_2B),[68] cobalt boride (CoB),[69] niobium boride (NbB_2),[70] and nickel boride (Ni_2B)[71] were synthesized from mixtures of micro-size boron and metal powders. It was demonstrated that their compositions, crystal structures, and sizes can be controlled by adjusting the ratio of boron to metal and the feeding rate.[64,67–69] The formation mechanism of various metal boride nanoparticles in an RF thermal plasma process (4 MHz, 101 kPa, 30 kW, B, Cr, Co, Fe, Mo, Nb, Ti, Ta, V precursors) was studied by Watanabe *et al.* Figure 5 shows the formation mechanism of metal boride nanoparticles in the thermal plasma flow subjected to rapid quenching.[68] The injected precursor mixture of metal and boron powder is evaporated at the high temperature region of the thermal plasma jet. As the temperature cools down, boron vapors reach the supersaturated state first due to their lower saturation vapor pressure compared to metals (except for niobium metal). Boron droplets form from the supersaturated vapors through homogenous nucleation and stay in a molten state until the temperature reaches their solidification limit around 2500 K. The calculated nucleation temperatures of each species in the feedstock showed that the nucleation temperature of boron is higher than most metals for the feeding rates and component ratios considered (see Fig. 6). The heterogeneous co-condensation of metal and boron monomers occurs on the surfaces of the boron droplets to form metal borides and these particles continue to grow through the coagulation process until they solidify. In their experiments,[69] it was found that a high feed rate of boron precursor resulted in a higher boron fraction in a particle with a larger crystalline diameter. This is because, due to

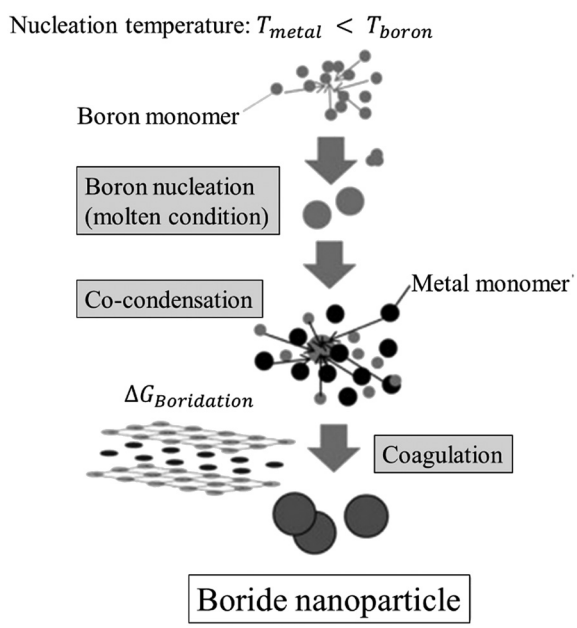

FIG. 5. Growth mechanism of metal boride nanoparticles from a mixture of boron and metal powders in an RF thermal plasma jet. Since the nucleation temperature of the metal is lower than that of boron, the heterogeneous co-condensation of metal monomers occurs on the surfaces of boron droplets to form metal borides. Reprinted with permission from Cheng *et al.*, Powder Technol. **246**, 210 (2013). Copyright 2013 Elsevier B.V.

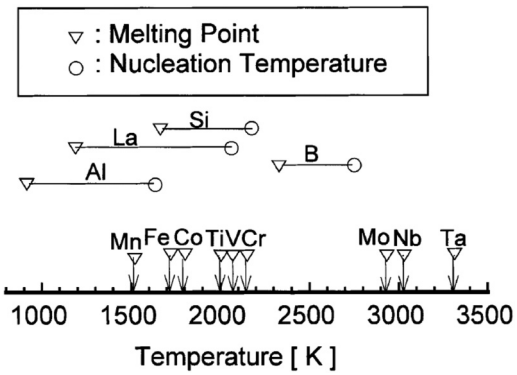

FIG. 6. Melting and estimated nucleation temperatures of boron and metals in the thermal plasma synthesis of various metal borides. Reprinted with permission from Watanabe *et al.*, Thin Solid Films **435**, 27 (2003). Copyright 2014 Elsevier B.V.

the higher vapor density, the nucleation temperature of boron elevated, extending the temperature gap between nucleation and melting temperatures of boron. Thus, particle growth time through co-condensation and coagulation was prolonged. The effect of boron-rich precursors can be understood in a similar way.

F. Composite materials

In thermal plasma processes, multiple atomic precursors are often employed to manufacture nanoparticles in a composite form by heterogeneous co-condensation or non-equilibrium condensation under a steep temperature gradient. Generally, they are produced as coated or core-shell structured nanoparticles and have binary properties of both seed and coated materials. Various composite nanoparticles including metal-metal,[72] metal-ceramic,[73–75] ceramic-ceramic,[76] and carbon-metal composites[77–81] were produced by the thermal plasma jet technology. Among them, metal-containing nanocomposite powders have many potential applications, such as a reinforced magnetic nanoparticle in magnetic data storage, battery, and biomedical drug and gene delivery applications. On the other hand, atomically thin layers of carbon or ceramics on a metal nanoparticle not only protect the metal core from corrosive environments but also provide additional chemical functionality. The oxidation, corrosion, and agglomeration problems of nano-size metal nanoparticles have been addressed by encapsulating them with relatively inert carbon or ceramic cages using thermal plasma jets.[80,81]

IV. SYNTHESIS OF LOW-DIMENSIONAL NANOMATERIALS

A. Carbon nanomaterials

Among various low-dimensional nanomaterials, carbon nanomaterials have been most widely studied in the past two decades. Related research has been largely boosted by the discoveries of carbon fullerenes (0D)[14] and nanotubes (1D)[15] in 1985 and 1991, respectively, and further expedited by the successful exfoliation of single-layered graphene sheet (2D)[16] and its characterization in 2004. Its capability to hybridize with different morphologies (e.g., sp^2 or sp^3 hybridizations) provides unique structure-dependent properties appealing to various applications including electronic devices, energy storage or converting devices, composites, and biomedicine.[82] However, their commercialization has been challenging due to the lack of technologies for mass production. High structural quality with crystal perfection also became a critical issue in exploiting their practical applications. Over the past two decades, thermal plasma jets have been proven to be capable of fast treatment of large quantities of feedstock in a continuous manner and also provide a unique processing condition such as *in situ* annealing; thus, they have been intensively studied for synthesis of various carbonaceous nanomaterials with low-dimensionalities.

1. Fullerenes

Fullerene is a closed-caged molecule composed entirely of pentagonal and hexagonal carbon rings. They were first synthesized in 1985 by irradiating laser beam on a graphite target under a helium atmosphere.[14] Their intriguing properties along with the hollow structure have attracted significant attention from a range of industry sectors including electronic, optical, biomedical, energy, and environmental sectors.[83] Arc discharges[84] were employed in the initial studies of their mass production but soon recognized not suitable for the production in quantity mainly due to the UV radiation and its batch mode operation. Upon scaling up the process, the UV radiation from the arc becomes more intense and enhances the photochemical decomposition of the fullerenes produced. It is crucial to transport the grown fullerenes away from the radiating arc zone to minimize the unwanted photochemistry. Thermal plasma jets provide a unique advantage over arc discharge that owing to their high jet speeds, rapid removal of the as-grown fullerenes from the arc zone is feasible minimizing their destruction by the UV irradiation.

There have been considerable attempts to synthesize fullerenes using the RF plasma technology. Wang *et al.*[85] employed an RF plasma jet (1.67 MHz, 30 kW, 10-20 kPa) to produce fullerenes from the direct evaporation of a mixture of carbon and silicon powders and found that silicon powder plays a role in enhancing the C_{60} yield by transforming the oxygen molecules coming from leaks to SiO_2, thus protecting the carbon sources from oxidation. Cota-Sanchez *et al.*[86] extensively investigated the effects of operating parameters (2-5 MHz, 20-40 kW, 40–66 kPa) and types of feedstock. Under the optimum condition identified (40 kW, 66 kPa, feed rate of 2 g/min), a fullerene yield of up to 7.7 wt. % was reported by using carbon blacks (CBs) as a carbon source. However, a mixture of CB-Fe and C_2Cl_4 demonstrated fullerene yields of 3.6 and 3.9 wt. %, respectively, and no fullerene was produced with C_2H_4. Todorovic-Markovic *et al.*[87,88]

investigated effects of physical properties of graphite powder feedstock (e.g., mean particle size, crystallinity) and helium content in the plasma gas on the fullerene formation. A fullerene yield of 4.1% was reported under the optimum conditions identified (3-5 MHz, 27 kW, 101 kPa, graphite feed rate: 2.6 g/min) noting that a highly crystalline feedstock improves the overall evaporation efficiency. This is due to their higher thermal conductivity which is crucial for the effective formation of fullerene precursors. Helium was also found to be favorable for the fast evaporation of graphite powder due to its higher thermal conductivity over that of Ar.

A DC-RF hybrid plasma torch is devised to expand a high-speed plasma jet ejected from a DC torch more broadly by applying an additional RF power at the bottom of the DC torch. Since fast and complete vaporization of carbon sources is one of the critical factors influencing the fullerene growth, a better yield was expected with a DC-RF hybrid plasma torch. Yoshie *et al.*[89] demonstrated the synthesis of fullerenes from carbon powder using a DC-RF hybrid plasma jet (4 MHz, 20 kW RF/5 kW DC, 35-101 kPa). A yield of about 7% was reported using carbon black, while a reduction of the reactor pressure to 35 kPa resulted in a decrement of the yield to 3%.

2. Carbon nanotubes (CNTs)

Carbon nanotubes (CNTs) are seamless cylinders of single- or few-layered graphene sheets and have been considered the ultimate material for advanced electronic, energy, composites, biomaterials, and optoelectronic applications due to their extraordinary physico-chemical properties.[90–92] Therefore, there have been numerous attempts to develop a cost-effective production method for CNTs including CVD, plasma enhanced CVD (PECVD), combustion, fluidized-bed catalytic CVD, arc discharge, and laser vaporization. Over the past decade, thermal plasma jets have also been intensively studied for the CNT synthesis and the main issues to address include structural quality and purity enhancement, scalability, and diameter or chirality control by changing plasma conditions and catalyst systems. The use of catalysts in CNT synthesis has been common to improve the yield and also to grow CNTs with a preferential structure. Transition metals (e.g., Fe, Ni, Co, Mo), which have a high carbon solubility, have been mostly employed.

Smiljanic *et al.*[93] reported the synthesis of single-walled carbon nanotubes (SWCNTs) from a mixture of ethylene and ferrocene by a microwave plasma jet (1300 W, 2.45 GHz, 101 kPa). This process was able to produce SWCNTs (1.5 nm in diameter) with reasonable structural quality. However, the main issue was that the plasma confinement tube was readily coated by electrically conductive carbonaceous deposits; thus, the plasma became unstable within 15–20 min losing the coupling with the microwave. DC plasma torches have also been employed in several studies.[94–98] Choi *et al.*[94,95] demonstrated the continuous synthesis of multi-walled CNTs (MWCNT, 30-60 nm in diameter, 1 μm in length) from methane decomposition [i.e., $CH_4 \rightarrow C(s) + 2H_2$, 1–4 slpm] using a non-transferred type DC plasma torch (350 A, Ar/H_2 plasma) and achieved a high purity (>90%). They found that the addition of 3.4% hydrogen in the plasma gas (Ar) greatly facilitated CNT growth by improving thermal conductivity and the enthalpy content of the plasma. This was crucial for the formation of nano-size metal particles (i.e., seeds for CNT nucleation) from the complete vaporization of the metal catalysts injected (Ni, 3 μm). Hahn *et al.*[96–98] reported the synthesis of high purity CNTs (~80%) from decomposition of carbon monoxide over iron particles with good controllability of the wall numbers by adjusting the feedstock injection position or hydrogen content. Despite their great potential to scale up, the crystallization degrees of the CNTs produced by DC plasma jets were relatively low mainly attributable to the short residence time of the reaction products in the hot zone due to the small hot volumes and high speeds of DC plasma jets.

In contrast to DC plasma torches, RF plasma torches generate plasma jets with larger hot volumes and lower speeds significantly extending the residence time of the feedstock or CNTs produced in the hot zone. Kim *et al.*[99,100] exploited the large-scale synthesis of SWCNTs from carbon black using an RF plasma (3 MHz, 40 kW, 66 kPa) and also studied the effects of carbon black grades, gas compositions, and metal catalysts on the SWCNT growth. A yield rate of 100 g/h was obtained with a high structural quality approaching that of laser-grown SWCNTs; however, its purity was relatively low estimated around 40 wt. %. The low purity obtained in the RF plasma process is mainly attributable to the incomplete vaporization of solid feedstock in the plasma. To minimize feedstock residue in the sample, Kim *et al.*[101] have further advanced the RF plasma process (2-5 MHz, 47 kW, 66 kPa) by employing liquid feedstocks (Fig. 7). In this new process, liquid hydrocarbons (e.g., toluene, C_7H_8, 40 mL/h) rather than solid carbons were employed through an atomizer with metallic catalysts (e.g., ferrocene with thiophene, 4 wt. %). The main advantage of using liquid feedstocks is that due to the lower evaporation energy of the liquid, it can achieve higher evaporation rate or treatment efficiency. Besides, liquid feedstock residue will not contaminate the main product as it will dry up during the process due to its high vapor pressure. Various material characterizations confirmed that the sample produced from this process consisted mainly of SWCNTs (1.2–2.5 nm in diameter) and the purity was improved to 50–60 wt. %. It was also found that addition of 10% H_2 to the Ar sheath gas improved the purity through the selective etching of amorphous carbons by hydrogen atoms.

The control of SWCNT diameter or chirality has been of particular interest especially in electronic applications. Kim *et al.*[101] also studied the effects of sulfur on the morphology of SWCNTs in the liquid feedstock process by varying the ratio between iron catalyst and sulfur (Fe:S = 1:1 and Fe:S = 10:1). Sulfur in an iron droplet lowers the melting point of the iron droplet by forming a Fe–FeS eutectic which serves as an active site for CNT growth. The size of this active spot is adjustable by controlling the sulfur content in an iron particle; with a higher sulfur concentration, this eutectic spot becomes larger through the aggregation of sulfur; thus, formation of larger diameter SWCNTs or MWCNTs was

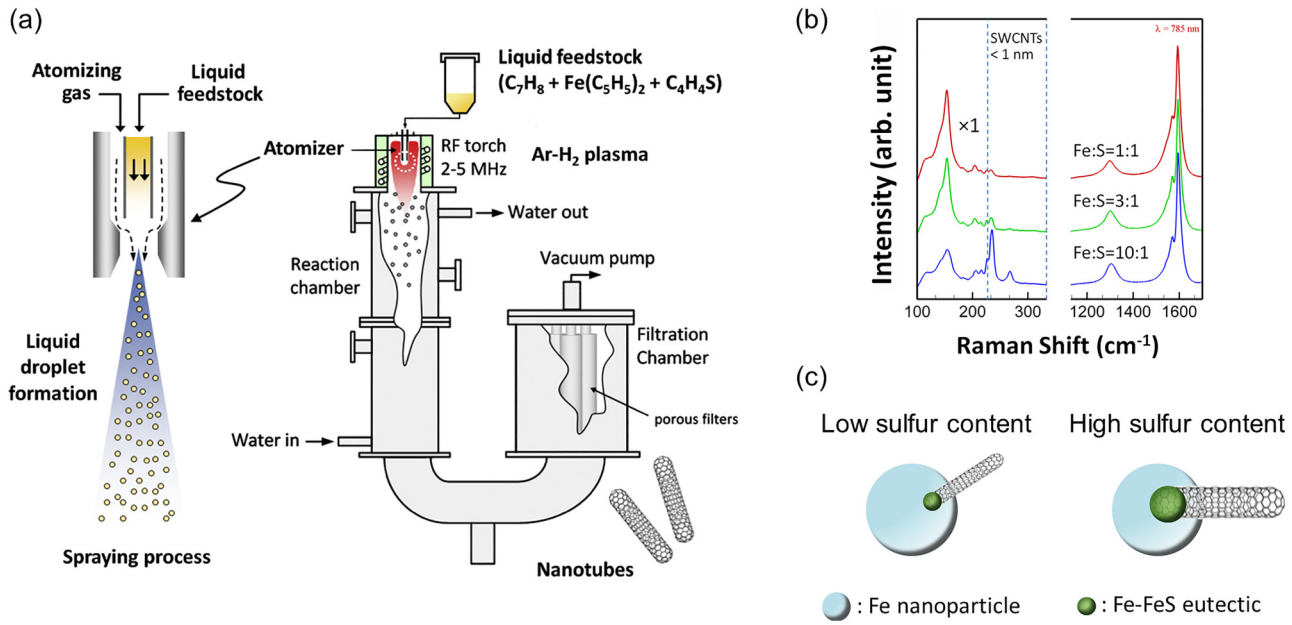

FIG. 7. Synthesis of single-walled carbon nanotubes (SWCNTs) from liquid hydrocarbon feedstock using an RF thermal plasma jet. (a) Schematic of the process. (b) Raman spectra of the SWCNTs produced showing the effect of the sulfur content on the diameter distribution of SWCNTs. (c) SWCNT diameter control mechanism by the control of the sulfur content in an iron metal catalyst. Reprinted with permission from Kim *et al.*, Chem. Eng. J. **250**, 331 (2014). Copyright 2014 Elsevier B.V.

expected [Figs. 7(b) and 7(c)]. In the synthesis experiments, it was found that large diameter SWCNTs (1.0–2.0 nm) were predominantly produced at a high sulfur content (Fe:S = 1:1) with a narrow chiral distribution, which is highly promising for the chiral pure synthesis of SWCNTs.

3. Graphene flakes (GFs)

Over the past decade, atomically thin 2D materials have drawn a great deal of interest due to their intriguing properties originating from the geometrical constraint in the out-of-plane direction. Among various 2D materials, graphene, a single layer of sp^2-hybridized carbon lattice has been extensively investigated due to its unusual electronic property that electrons in graphene behave like massless Dirac fermions.[102] This new property is expected to make a transformative impact to many applications ranging from electronics to energy and biological applications.[103] Graphene has been prepared by various methods including micromechanical cleavage of bulk graphite (e.g., by scotch tape or ball milling), CVD on metal substrates, chemical exfoliation, and solvothermal methods. Despite impressive advancements in this field, production of large quantities of graphene with good control of defect, grain size, number of layers, and crystallographic stacking order still remains key challenges. Considerable attempts have been made to fabricate graphenes using thermal plasma jets as well as by taking advantage of their continuous processing capability and high temperatures. In those attempts, most of the materials were synthesized in gas-phase without a supporting substrate; thus, the processes resulted in the production of crumpled, few-walled graphene flakes (GFs).

Kim *et al.*[104] reported a synthesis of GFs from the thermal decomposition of methane (20 L/min) using a DC plasma torch with hollow electrodes that operated in a reversed polarity mode (48 kW, 101 kPa, Ar). The custom-built plasma torch had a pilot electrode to extend the arc column. This allowed for radial injection of the feedstock directly into the arc column improving the dissociation efficiency. The size of the GFs synthesized ranged from 100 to 150 nm and their average thickness was about 10 nm. The material analyses indicated excellent physico-chemical properties, such as a large specific surface area and a highly crystalline structure. Interestingly, a similar process using a DC-RF plasma torch produced spherical graphitic carbons (i.e., carbon black).[105] It was speculated that the high temperature with strong directional flow inside the DC torch may play an important role in the anisotropic growth of graphitic materials with a high crystallinity. A DC torch with a rod-type cathode (200 A) was also used to fabricate high quality GFs.[106] In this process, a carbon atomic beam was formed by injecting ethanol (0.01–1 mL/min) into an Ar plasma jet. The atomic beam was further guided downstream by a carbon tube (0.5 cm in diameter, 20–30 cm in length) attached to an anode (Cu, 0.6 cm in diameter) and eventually impinged on a graphite plate where GFs were formed via epitaxial growth. Thus, the surface crystalline

structure of the graphite plate dictated the crystalline structure of the GFs formed. It was also noted that reducing the speed of the carbon beam to a proper range using the carbon tube is critical to produce GFs rather than CNTs or amorphous carbons. The GFs fabricated was pure with a relatively good crystallinity.

Pristavita *et al.*[107,108] reported the GFs synthesis from methane precursor (0.5–5 L/min) using an RF plasma torch (~3 MHz, 20 kW, 55.2 and 89.6 kPa) for catalyst applications (Fig. 8). A conical reactor was used for the gradual expansion of the plasma jet to avoid rapid quenching of the reaction stream by recirculation eddies. This controlled flow pattern promoted the formation of GFs with a uniform morphology (100 nm long, 50 nm wide, and 5 nm thick) while suppressing the formation of impurities. A synthesis of N-doped graphene (0.69 at. % in the form of a pyridinic type of N-bonding) was also successfully demonstrated by adding nitrogen which is highly desired for fuel cell applications. Meunier *et al.*[109] reported a numerical simulation of this process to understand the GF formation mechanism by studying the effects of operating conditions (e.g., power, pressure) on the nucleation temperature and quenching rate [Figs. 8(b) and 8(c)]. A recent study of a similar RF process showed that addition of a small amount of H_2 (~0.3%) into an Ar plasma jet promoted the growth of GFs.[110] It was argued that hydrogen atoms produced at high temperatures (>3500 K) terminate the dangling bonds on the edge of GFs, thus prevent the GFs from folding into closed structures such as carbon onions or carbon blacks. Amorphous carbons could also be etched by reactive hydrogen atoms.

Natural bulk graphite is composed of many graphene layers bonded by the relatively weak vdW force, thus can be a good source for fabricating GFs in an economically way through chemical or mechanical exfoliations. Such a top-down

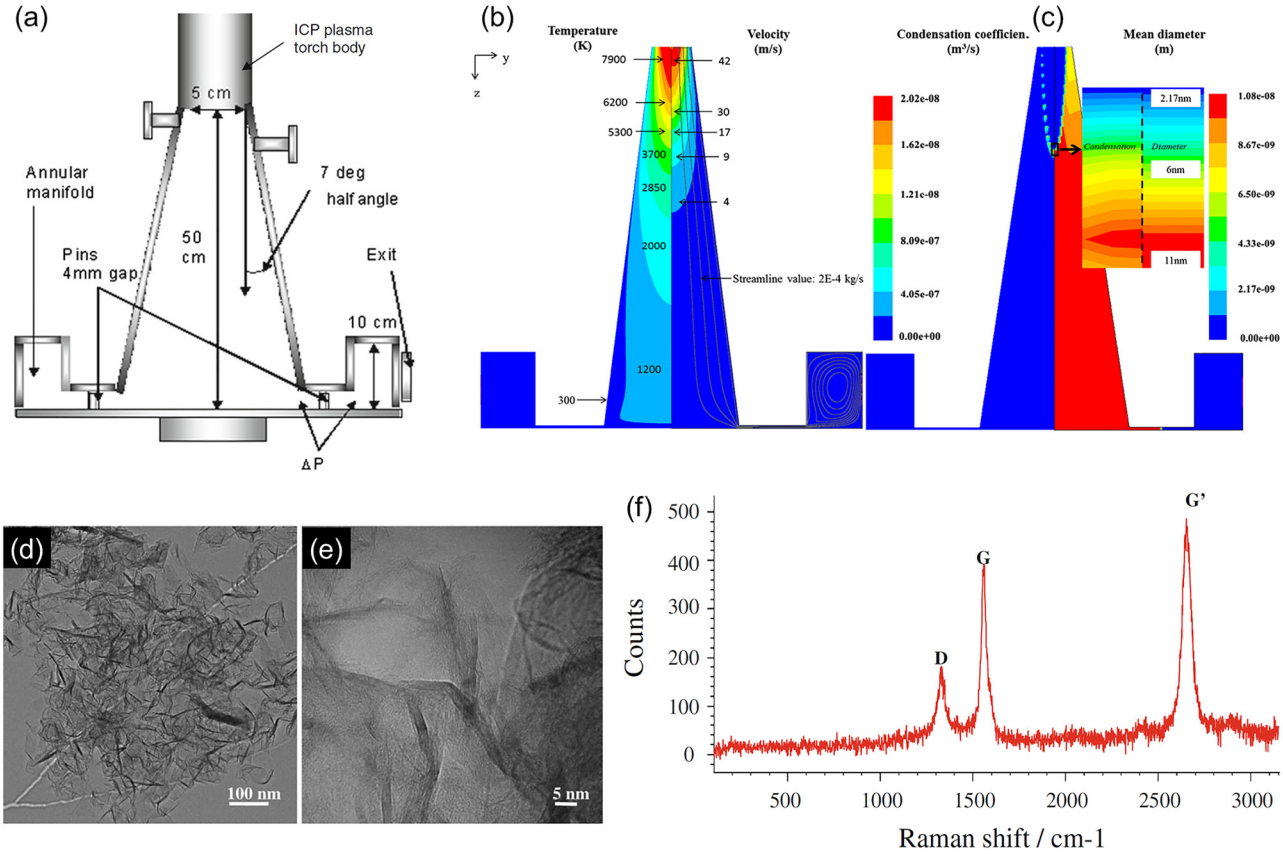

FIG. 8. Synthesis of graphene flakes (GFs) by an RF thermal plasma jet. (a) Schematic of the process. Numerical modeling of the process showing distributions of (b) thermofluid (left: temperature, right: velocity) and (c) particle fields (left: condensation coefficient, right: particle mean diameter). The streamlines in (b) show the absence of recirculation eddies at the entrance of the reactor which promoted the GF formation with a uniform morphology. (d) and (e) TEM images of the GFs produced. The layered structure of graphene is seen in (e). (f) Raman spectrum of the GFs produced. The strong G′ peak at 2680 cm^{-1} confirms the existence of GFs in the sample. Reprinted with permission from Pristavita *et al.*, Plasma Chem. Plasma Process. **31**, 393 (2011). Copyright 2011 Springer Science+Business Media and Meunier *et al.*, Plasma Chem. Plasma Process. **34**, 505 (2014). Copyright 2014 Springer Science+Business Media.

approach has also been explored by using a thermal plasma jet. This process involved chemical intercalation of bulk graphite using nitric or sulfuric acids, followed by its rapid thermal expansion in a thermal plasma jet (RF plasma, 90 kW) at a temperature above 5000 K.[111] Upon applying the extreme thermal shock, some of the individual graphene layers were separate and formed nano-platelets. This provided a cost-effective route to produce GFs in commercial quantities, the production rate demonstrated being 10 kg/h. It was also found that a plasma gas containing oxygen is favorable for obtaining a higher expansion factor and specific surface area over other inert gases.

4. Graphene quantum dots (GQDs)

Graphene has a fatal drawback in its electronic and optoelectronic applications that it has a zero bandgap. This greatly limits its uses in many electronic or optical device applications. Graphene quantum dots (GQDs) are graphene sheets with lateral dimensions less than 100 nm; thus, they exhibit strong edge effects as well as quantum confinement effect in the in-plane direction.[112] This difference allows bandgaps of GQDs suitable for the fabrication of nanoscale electronic, optical, and bio-imaging devices. The DC plasma process developed for the GFs synthesis has been modified for the growth of GQDs whose sizes are less than 20 nm with a relatively narrow size distribution (Fig. 9).[113] In this process, a carbon-containing atomic beam was produced by injecting ethylene gas (2.5 L/min) into an Ar plasma jet (12 kW) but directly discharged into a chamber through a carbon tube (5–20 cm in length, 2 cm in diameter) without the graphite plate employed in the previous GFs synthesis. Thus, GQDs grow from gas phase collision of the carbon atomic beam in the carbon tube, limiting their continuous growth to larger-scale GFs. The carbon soot produced contained about 10% GQDs which is equivalent to a production rate of 4 g/h. It was also noted that the size of GQDs was controllable from 10 to 19 nm by changing the length of the carbon tube attached. Various characterizations indicated that the GQDs produced were terminated by carbyne-like edges which improved their solubility in various organic solvents.

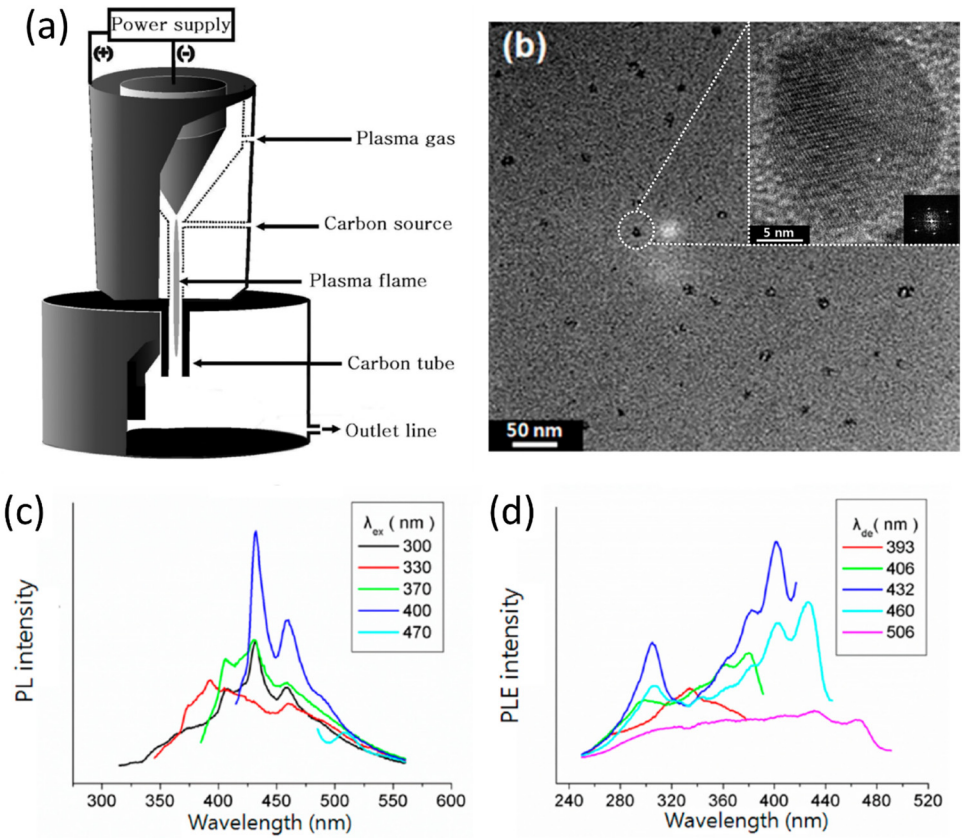

FIG. 9. Size-controllable synthesis of graphene quantum dots (GQDs) using a DC thermal plasma jet. (a) Schematic of the process. (b) TEM image of the GQDs produced. (c) Photo-luminescence (PL) emission and (d) excitation spectra of 19 nm GQDs. Reprinted with permission from Kim and Suh, ACS Nano **8**, 4190 (2014). Copyright 2014 American Chemical Society.

B. Hexagonal boron nitride (hBN) nanomaterials

The progress in the synthesis of carbon nanomaterials has intrigued the study of analogous nanostructures of various inorganic compounds. Among them, the hexagonal boron nitride (hBN) system composed of sp^2-lattices with alternating B and N atoms has been of particular interest as it is also known to form tubular (1D) or atomically-thin layered (2D) structures at the nanoscale. In the past two decades, its nanostructures, such as boron nitride nanotube (BNNT) and nanocage (BNNC), have emerged as a new class of nanomaterials presenting new properties complementary to those of carbon nanomaterials. Unlike carbon nanomaterials, they are wide bandgap semiconductors (~6.0 eV) and transparent in the visible spectrum with a remarkable thermal stability in air up to 900 °C, electrical insulation with high thermal conductivity, thermal neutron absorption ability (767 barns), single-photon emission, and piezoelectricity.[114–116] Very recently, the thermal plasma jet technology has also demonstrated great potential for the large-scale synthesis of BN nanostructures with high structural quality which led to their successful commercialization.

1. Boron nitride nanotubes (BNNTs)

Boron nitride nanotubes (BNNTs) are rolled-up cylinders of single- or few-layered hBN sheets which consist of alternating boron and nitrogen atoms in a hexagonal lattice.[117] Structurally, they are close analogs of CNTs; thus, BNNTs possess exceptional mechanical strength comparable to that of CNTs. However, they have other properties as described above which makes BNNTs a better fit than CNTs for applications under harsh conditions such as high-temperature, oxidative, and radioactive environments.[114–116,118]

Despite their relatively early synthesis in 1995,[119] large-quantity production of BNNTs with high quality and purity still remains a challenge mainly due to the heteroatomic nature of BN, limited access to boron sources, and needs for extreme synthesis conditions (e.g., high temperatures and high pressures).[120] Among the various synthesis methods studied, high-temperature methods including arc discharges[119] and laser vaporizations[121] made good headway toward manufacturing of highly crystalline, small-diameter BNNTs (<10 nm) from the direct vaporization of pure B or BN sources.[120] In those processes, boron droplets are produced from the dissociation of the feedstock mixture and subsequently react with N-containing species such as N_2 to form BN phases on the surfaces of the boron droplets. The spherical geometry of the boron droplets guides the growth of the BN network into a tubular structure (i.e., BNNT). Thus, in those processes, the BNNT growth rate is largely dictated by the speed of the in-flight reaction between boron droplets and N-containing species. However, the direct B-N_2 reaction at atmospheric pressure is known to be extremely slow due to the strong triple bond of N_2.[122] Nitrogen radicals are also produced by the high temperature arc or laser but recombined into N_2 molecules at a high temperature of 7000 K, thus, mostly not available in the temperature range suitable for the boron droplet formation (<4000 K). This greatly limits BNNT growth in those processes, a typical yield rate being less than 1 g/h. This may require a high N_2 pressure to increase the collision frequency between boron droplets and N_2 molecules.[123]

Very recently, Kim *et al.*[124] at the National Research Council Canada reported the scalable manufacturing of BNNTs directly from hBN powder (70 nm) using RF plasma (2-4 MHz, 50 kW, $Ar/H_2/N_2$ plasma, 93 kPa) as a heat source and hydrogen (13%) as a catalyst (Fig. 10). This new plasma process demonstrated that in the presence of hydrogen, high-yield growth of BNNTs (~20 g/h) is possible even at atmospheric pressure and was named as hydrogen-catalyzed BNNT synthesis (HABS). In the follow-up study,[125] the detailed role of hydrogen was investigated both by computational fluid dynamics (CFD) simulations and *in situ* optical emission spectroscopy (OES). The numerical simulation suggested enhanced particle heating and quenching rates (~10^5 K/s) by the improved thermal conductivity due to hydrogen. This is important for the complete vaporization of hBN feedstock and rapid formation of B droplets (i.e., BNNT nucleation sites), respectively. The OES study observed that the presence of hydrogen promotes the formation of good BN precursors such as NH ($A^3\Pi$–$X^3\Sigma$) and BH ($A^1\Pi$–$X^1\Sigma$) radicals while suppressing the recombination of freed N radicals into N_2 [Fig. 10(f)]. Compared to inert N_2, such species can easily release B or N species to boron droplets owing to relatively weak bonds of N-H or B-H, respectively.[125] A detailed study of the roles of such B-N-H containing species was also reported by Krstic *et al.*[126] using quantum-classical molecular dynamic (QCMD) simulations in support of this experimental work. A similar RF plasma process at high pressures (extended-pressure inductively-coupled plasma, EPIC, >300 kPa) was also reported demonstrating a high production rate of 35 g/h without using hydrogen.[127]

2. Boron nitride nanocage (BNNC)

Fullerene-like structure at the nanoscale is not limited to carbon species. BN nanocages (BNNC) have also been attracting significant attention owing to their hollow structure, low density, and corrosion resistivity which are highly appealing to many applications such as containers for delivery of drugs or hydrogen storage. Their high mechanical strength with weak interlayer bonds (i.e., vdW type interaction) can also find important applications in nanotribology by reducing the resistance to shearing forces (e.g., nanoscale lubricants). BNNCs have been commonly reported as by-products in BNNT synthesis by arc discharges or laser ablations.[128] Some solution-based or solid-state methods have also been developed to produce BNNCs or BN nano-polyhedrons using polymeric BN precursors such as borazine or metal catalysts;[129] however, the preparation of small-diameter BN cages (<50 nm) with wall numbers less than 5 still remains a significant challenge to date.

The RF plasma processes developed for BNNT synthesis have turned out to be highly efficient for the synthesis of BNNCs by controlling the reaction rate between boron

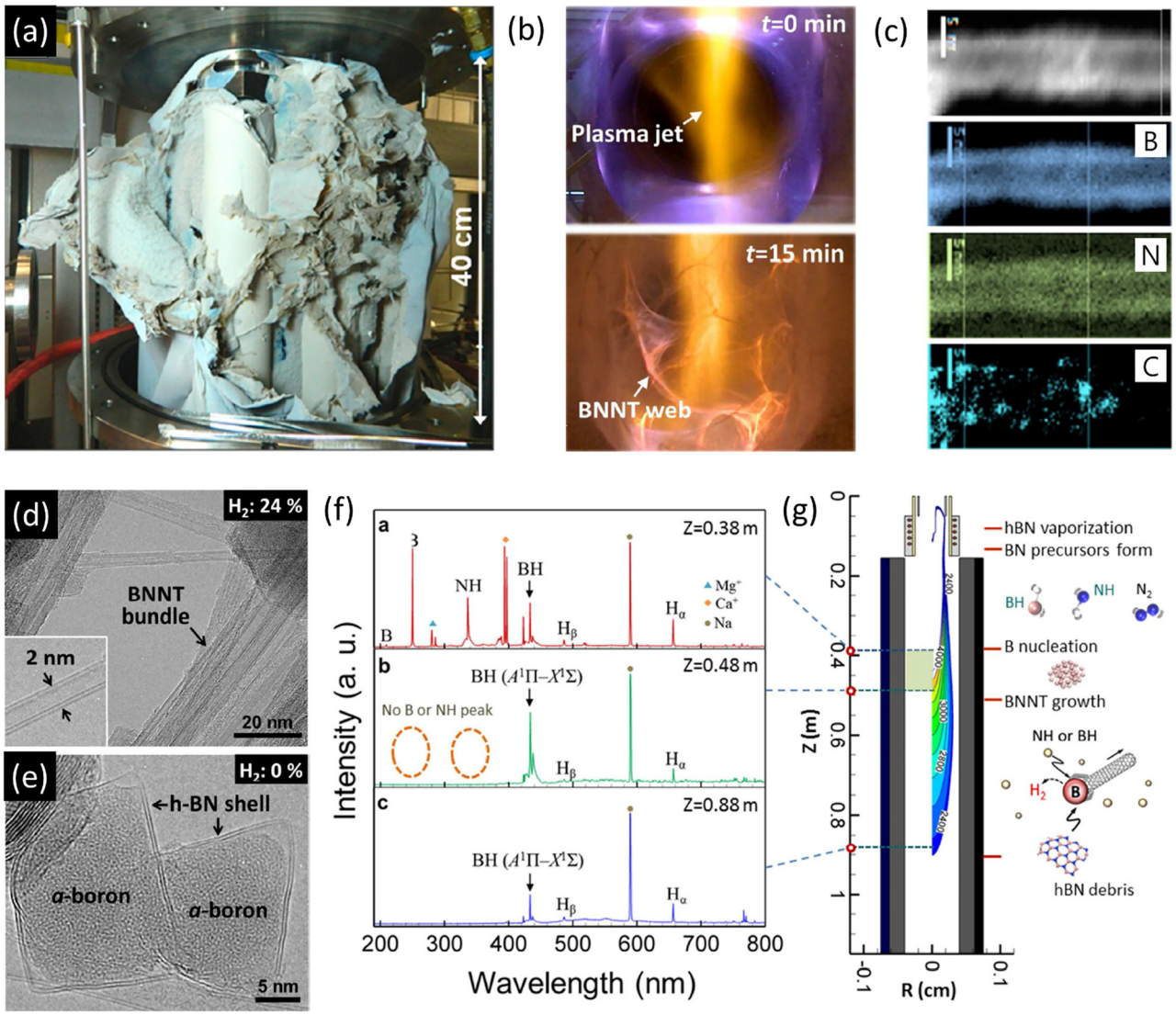

FIG. 10. Large-scale synthesis of hexagonal boron nitride (hBN) nanomaterials by an RF thermal plasma jet. (a) Photo of the boron nitride nanotube (BNNT) materials grown with the assistant of hydrogen. (b) Photos of the BNNT webs formed inside the reactor after 15 min. (c) Zero-loss energy-filtered image of a BNNT and its elemental maps. (d) TEM image of BNNTs. (e) TEM image of boron nanoparticles encapsulated with hBN shells. They were produced in the absence of hydrogen in the plasma gas. (f) Optical emission spectra showing the spatial evolution of chemical species during the BNNT synthesis. (g) BNNT growth mechanism proposed for the hydrogen-assisted BNNT synthesis. Reprinted with permission from Kim *et al.*, ACS Nano **8**, 6211 (2014). Copyright 2014 American Chemical Society and Kim *et al.*, ACS Nano **12**, 884 (2018). Copyright 2018 American Chemical Society.

droplets and N_2. By either removing hydrogen in the HABS process[125] or reducing the operating pressure (<200 kPa) in the EPIC process,[127] it was reported that boron nanoparticles encapsulated with hBN shells were predominantly produced rather than BNNTs [Fig. 10(e)]. Under such conditions, the reaction rate between boron droplets and N_2 is not high enough to form BNNTs. The amorphous boron in the core can be easily leached out by acids leaving the BN shells behind to produce BNNCs. This allows for the production of small-diameter BNNCs (<50 nm) in quantity with small wall numbers (<5 walls).

C. Other low-dimensional nanomaterials

There are other different types of layered materials beyond "C and hBN systems" available for the study of

fabrication of 1D or 2D nanomaterials. Such materials include TMDCs, black phosphorus, and borophene and can also find their important applications in science and technology. Syntheses of other types of inorganic nanotubes, such as WS_2, MoS_2, and TiO_2, have been reported in the literature along with their 2D counterparts.[130] Although low-temperature plasmas have been routinely employed for their synthesis,[131] thermal plasma jets have been less studied in this area; thus, considerable opportunities still remain.

Nanowires are also interesting 1D nanomaterials with high aspect ratios of 1000 or more and can be an important building block in a wide range of applications in nano-science and technology. Zinc oxide (ZnO) is a n-type semiconductor material with a direct band of about 3.2 eV and mostly stable in the form of hexagonal wurtzite structure. A DC thermal plasma (90 kW, air carrier gas) has been employed to produce ZnO nanorods (30 nm in diameter, 100–200 nm in length) from Zn powders (10 μm).[132] Nanowires of cubic aluminum nitride (AlN) were also synthesized by DC arc-plasma-induced melting of aluminum in a nitrogen–argon ambient.[133] Very recently, silicon nanoparticles and nanowires were successfully produced from silicon powder (19.2 μm) by a pulse-modulated RF plasma torch (20 kW, 40 kPa, Ar-H_2 plasma, modulation at 80% shimmer current level and 80% duty factor) which allows effective control of thermofluid and chemical species fields through an amplitude modulation of the coil current (Fig. 11).[134] In this new process, silicon nanoparticles (10–30 nm) were mainly synthesized with an intermittent feeding (<4 g/min) in the presence of quenching gas (Ar, 50 L/min), while many silicon nanowires (mean diameter of 14.7 nm) were produced with a heavy loading of feedstock (~7 g/min) in the absence of quenching gas. It was noted that the high production rate of silicon nanowires (>1 g/h) is attributable to the generation of high-density silicon vapor and a moderate temperature gradient along the reactor axis. The detailed growth mechanism is under investigation.

V. FUTURE OUTLOOK

Thanks to new properties emerging from their high surface-to-volume ratio and quantum confinement effects, nanomaterials have presented a great potential in diverse areas of science and technology; thus, their economically viable and reliable synthesis has been of particular interest. Despite the significant advancements of the related research fields, large-scale production of quality nanomaterials still faces many challenges and is seeking new synthesis methods. In the past two decades, thermal plasma jets have demonstrated great potential as an important fabrication tool for various nanomaterials from nano-sized particles to low-dimensional nanomaterials via both bottom-up and top-down approaches. Thermal plasma jets have offered a unique processing environment, such as high temperatures with strong spatial gradients, high chemical activity, short processing time, and good controllability of the thermofluid fields that have been difficult to achieve by other conventional approaches.

Recent progress in nanofabrication based on thermal plasma jet technology is highly encouraging; however, low conversion rates and uncontrolled structural (e.g., diameter, chirality, and wall numbers) or compositional properties are still key challenges in further exploitation of nanomaterials synthesis. Further advancements in this field increasingly rely

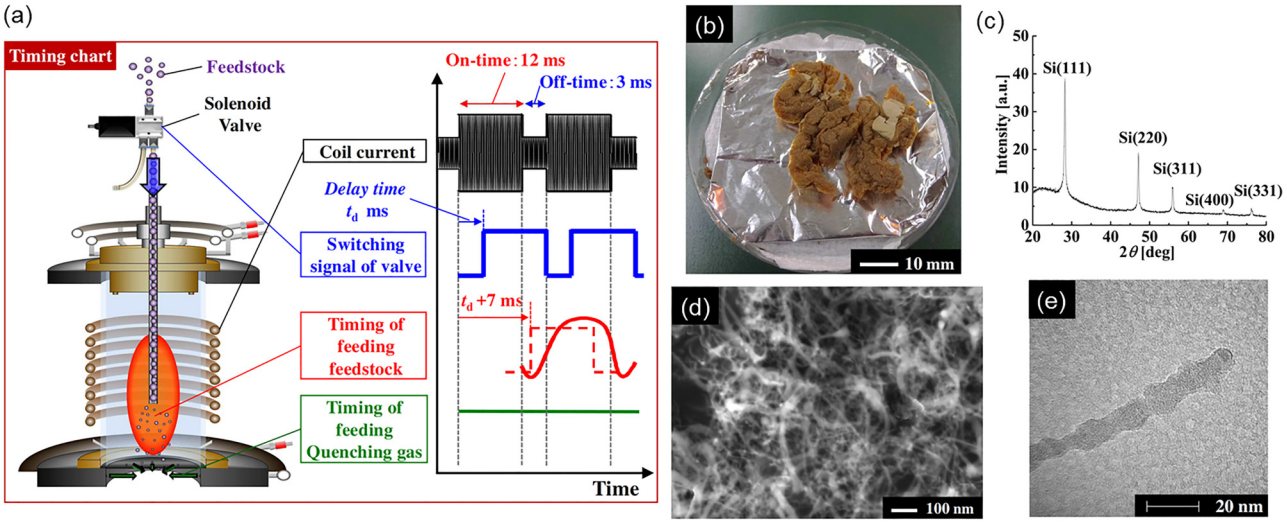

FIG. 11. Scalable synthesis of silicon nanowires by a pulse-modulated induction thermal plasma (PM-ITP) jet. (a) Schematic of the process. (b) Photo of the as-produced samples. (c) X-ray diffraction spectrum. (d) FE-SEM image of silicon nanowires. (d) TEM image of a silicon nanowire. Reprinted with permission from Ishisaka *et al.*, "Large amount synthesis of Si nanopowder/nanowires using pulse-modulated induction thermal plasmas," Reprinted with permission from Ishisaka *et al.*, Appl. Phys. Express **10**, 096201 (2017). Copyright 2017 The Japan Society of Applied Physics.

on the understanding of the nucleation and growth mechanisms of nanomaterials under various plasma jet conditions. However, the extreme processing conditions of plasma jets (e.g., high temperatures, steep gradients in thermofluid and chemical fields, non-equilibrium) that enable the production of exotic nanomaterials often create an environment difficult to understand or monitor the process. To aid in the comprehensive understanding of nanomaterial growth by thermal plasma jets, ongoing research effort is focused on developing and advancing numerical models and diagnostic techniques via multidisciplinary approaches. In Secs. V A and V B, we will discuss progress in those areas as well as identifying the key challenges and close this Perspective with a brief introduction to synthesis of new revolutionary nanomaterials where unique advantages of thermal plasma jets may exist.

A. Modeling of nanomaterial growth by thermal plasma jets

As the thermal plasma synthesis of nanomaterials becomes more viable, there has been a pressing demand for the development of a numerical model to better understand the process.[135] While this will require a computational model with an elevated accuracy and completeness, manufacturing of nanomaterials by plasma jets is a very complicated process involving multi-phase plasma generation, fast heat and mass transfer, turbulent flows, chemical reactions at high temperatures, and nanostructure formation and growth.[135,136] Besides, the process is intrinsically dictated by atomic or molecular processes (e.g., nucleation, co-condensation, coagulation) that are affected by macroscopic parameters (i.e., thermofluid fields) describable by a continuum approach. Thus, an "atomistic-to-continuum scale modeling" technique is needed to bridge the gap between the phenomena occurring at different length scales.[12]

In the past two decades, 2D self-consistent numerical models based on the CFD and aerosol dynamics have been developed to simulate the nucleation and growth of nanomaterials in thermal plasmas.[137–141] These multi-scale and multi-phase models include various physico-chemical processes occurring at different scales: (1) plasma generation, (2) plasma-material interaction via heat and mass transfer, (3) nucleation of small clusters from supersaturated vapors, and (4) nanomaterial growth through co-condensation and coagulation. The plasma generation and its interaction with feedstock were described by the magneto-hydrodynamic (MHD) equations (i.e., a set of the conservation equations with electromagnetic Maxwell equations) and the particle-source-in-cell (PSI-CELL) approach,[142] respectively. Nanoparticle formation through homogeneous nucleation,[143,144] co-condensation, and coagulation were taken into account by solving the general dynamic equation (GDE) using the method of moment (MoM) with an assumption of a log-normal particle size distribution[137–139] or nodal methods.[140] By using these numerical models, it has been possible to predict the mean particle size or length of nanomaterials that agrees with the experimental observations.[141]

Despite this progress, there is still a need for improvement. Recently, liquid feedstock or submerged plasma jets generate a new interest in nanofabrication by plasma jets because the liquid usually requires lower vaporization energy compared to the solid and also provides additional active chemical species from its dissociation.[145] However, its interaction with plasma is very complicated involving multi-phase plasma generation, thus not well understood. A fundamental understanding will be needed to model droplet formation, vaporization, dissociation, ionization in liquids, and gas-liquid interfacial areas.[145] As the chemical composition in the present plasma process becomes more complicated, there is a great demand on the development of plasma chemistry models to map out possible reaction pathways including formation of intermediate species at high temperatures. For such simulations, a complete set of thermodynamic and transport data for various chemical species will be needed for a wide range of temperature. Multicomponent nucleation/co-condensation should also be taken into account accordingly by a refinement of current homogeneous nucleation theory[143,144] and single component co-condensation models.[146,147] The nucleation and growth of nanoparticles are inherently atomic-scale processes; thus, it is very difficult to model anisotropic structural evolution of nanomaterials using solely the continuum approach.[109] Atomistic-scale simulations by the first principle methods, such as density functional theory (DFT) or molecular dynamic (MD) simulations, will be needed together with CFD simulations.[148] Lastly, the prediction of aggregation of nanomaterials with specific morphology or formation of internal or hierarchical structures (e.g., core-shell, multi-layer) is also an important research area because such details will affect performance of nanomaterials at macroscopic scales. In this case, particle charging will play an important role requiring a model that can estimate the plasma potential accurately and also capture two-temperature non-equilibrium effects.[149–152]

Detailed modeling studies of precursor evaporation, transport, and nanoparticle formation in RF plasma jets have expedited progress in optimization and commercialization of the synthesis of various nanoparticles by RF thermal plasmas.[135] Fundamental understanding of transport phenomena under different plasma conditions improved our capability to predict the impact of particle loading on the thermal and flow fields and their subsequent influence on the efficiency of the treatment of the feedstock.[135] Researchers can also leverage this progress toward the modeling of low-dimensional nanomaterials by thermal plasmas to make a similar progress in CNT or BNNT synthesis.[99,124] However, the challenges discussed above are more prominent in this case.

The growth rate is one of the parameters of particular interest in a real process. It is well documented that the nanotube formation begins from the adsorption of precursor atoms or molecules on the surface of catalyst nanoparticles (e.g., metal nanoparticles in the CNT growth while boron droplets in the BNNT growth), followed by the nanotube nucleation through surface precipitation or reactions of the adsorbed precursors.[153] Therefore, the detailed interaction between catalyst particles and precursor species at the atomic scale must be described properly to accurately estimate the

nanotube growth rate. To date, a two-step computational strategy has been employed to simulate the nanotube growth kinetics: the CFD simulation predicts the thermal flow and nanoparticle fields in the reacting flow, and then, information, such as number density of nanoparticles, volume fraction of gas-phase precursors, and temperature gradient was incorporated to a simple kinetic model for the estimation of the growth rate.[141] Therefore, this approach neglects the changes in the plasma properties (e.g., local temperature and species concentration) due to the nanotube growth. A self-consistent, multi-scale modeling that couples the two different length scales is needed to accurately predict the catalytic growth of nanotubes in the thermal plasma jet.

Accurate information of species composition and their thermodynamic properties and transport coefficients is critical to reliable numerical simulations. Carbon–argon and carbon–helium mixtures have been extensively used in the CNT or graphene synthesis by thermal plasmas; thus, data are relatively well documented for those mixtures and accessible in the literature.[154,155] Most of CNT syntheses employ metal particles as well as in the feedstock mixture, to promote nanotube growth.[153] It is well documented by Murphy and his co-workers that the presence of metal vapors even at a very small amount alters the plasma properties substantially: it may lead to cooling of the plasma plume due to enhanced radiative heat transfer and also increase the electrical conductivity at lower temperatures due to their low ionization potentials.[156] Although these changes are likely to affect the energy transfer during the nanotube growth, the effects of metal vapors have not been considered in the previous nanotube synthesis modeling due to the absence of transport data such as net emission coefficients.

On the other hand, the B-N or B-N-H system has been commonly studied in BNNT synthesis,[124,127] thus the chemical composition being more complicated than the CNT case. Thermodynamic and transport data of those systems are rarely accessible in the literature for a broad range of temperatures. Transport properties of gas-phase species can be calculated as functions of collision cross sections (collision kernel) and temperature. Since collision cross sections for the B-N system are unknown, in the literature, collision cross sections of a similar system (e.g., C-N system) were approximated using appropriate molecular weights.[157] This may cause a substantial error in predicting the growth rate of BNNTs. Lastly, once nanotubes are grown from catalyst nanoparticles, the spherical particle assumption on the particle morphology is no longer valid. Since transport phenomena of non-spherical particles with high aspect ratios should be different from those of spherical ones, the development of collision dynamics of non-spherical particles should be of critical importance to simulation of their transport and aggregation.[158]

In a real process, a high flux of quenching gas or high loading of feedstock can cause the plasma to deviate from chemical or thermal equilibrium.[159,160] Modeling work by Tanaka showed that the non-equilibrium effects should be considered for accurate prediction of the species and temperature fields in the Ar-N_2 plasma generated at atmospheric pressure.[160] Chemically, non-equilibrium simulation is not only important for accurate calculation of thermodynamic and transport properties of the plasma but also critical to the identification of important precursors in the early stage of the nanomaterial nucleation. While a detailed chemistry simulation has been reported for the SWCNT synthesis in an RF plasma reactor predicting the formation of metal, carbon clusters, and SWCNTs,[161] no attempt has been made for BNNT synthesis. Recent thermodynamic equilibrium calculations of B-N and B-N-H systems suggested that B_2N would be an abundant and active precursor for the BNNT growth in the absence of hydrogen.[162] Although the presence of B_2N was verified by optical emission spectroscopy, a discrepancy also existed between calculated and measured results suggesting the chemically non-equilibrium condition prevails in a real process. A detailed chemistry simulation considering finite reaction rates and diffusion/convection effects is highly desirable to confirm this new finding in the BNNT synthesis. The thermally non-equilibrium condition (i.e., a two temperature plasma, $T_e \neq T_{\text{heavy particle}}$) may also affect the structure of the nanotubes grown from nanoparticles. In this case, the electron density is higher than that of the equilibrium case for a given temperature; thus, the charging density of nanoparticles may increase.[160] This could suppress the growth of nanoparticles by reducing the collision rate due to the repulsive Coulomb force. Since nanotube diameter is largely dictated by the size of catalyst nanoparticles, the thermally non-equilibrium condition should be taken into account properly to accurately predict the nanotube structures such as diameter.

B. Diagnostics of nanomaterial nucleation and growth

Utilizing *ex situ* characterization techniques such as TEM, SEM, X-ray diffraction, XPS, or Raman spectroscopy has facilitated the progress toward understanding nucleation and growth mechanisms of nanomaterials by various synthesis methods. However, *in situ* studies of nanomaterial growth can provide a more critical insight into synthesis mechanisms revealing information that has not been accessible through *ex situ* routes. Besides, numerical models developed need to be validated with *in situ* measurements of thermofluid or species fields, particle nucleation, and growth rates. For instance, the detachment of a sp^2-carbon cap from the surface of a catalyst particle is a critical process in the early stage of the nanotube nucleation and growth. The direct observation of this event in the CVD process has been studied *in situ* by an environmental transmission electron microscope (ETEM) and revealed dynamic reshaping or reconstruction of catalyst surfaces in detail during the SWCNT synthesis.[163,164] This direct observation led to an understanding of the driving force of CNT nucleation and also provided a basis of continuum or atomistic simulations of the process. A similar study is highly desirable for the process by thermal plasmas; however, the conditions (e.g., ultrahigh vacuum, low temperature) within an ETEM are far from the real conditions employed in a typical thermal plasma process.

Various technologies have already been developed for the *in situ* characterization of a thermal plasma jet alone including optical emission spectroscopy (OES), absorption spectroscopy, laser-scattering methods, and enthalpy probe measurement.[165] Such techniques can also be directly applied to the basic characterization of plasma properties during nanomaterials synthesis, while development of new diagnostic methods will be needed to map out the growth kinetics of nanomaterials by monitoring the chaotic interactions between plasma and materials, rapid phase transitions (e.g., vaporization and nucleation), and chemical reactions at high temperatures. Synthesis of nanomaterials by thermal plasma starts with the precursor formation via vaporization or dissociation of feedstock. A detailed knowledge on the precursor formation and their kinetics is crucial for the understanding of the early stage of the process. This requires measurements of ionic and radical species with methods such as OES, absorption spectroscopy, laser-scattering methods, or mass spectroscopy. Recent progress includes some characterization by OES and laser induced fluorescence (LIF) techniques which have been successfully applied for the detection of important precursors in the CNT and BNNT synthesis to reveal their critical roles in the fast growth of those nanomaterials.[125,166]

To investigate the growth of nanomaterials, it is important to probe small clusters or nano-size debris (<few nm) which serve as the nucleation sites of nanomaterials. Effective measurements of those small particles will largely rely on the existence of their suitably strong fingerprint signals with reasonable spatial/signal resolution. Techniques to detect micro-size particles are well established using laser-scattering methods and relevant information has been well documented.[167] However, for very small particles below few nm (e.g., seed or precursor for nanomaterial growth), light scattering may be inefficient and may require development of new particle probing techniques. Recently, it is proposed that a laser-based technique (e.g., coherent Rayleigh-Brillouin scattering, CRBS) can be used to detect nanoparticles with characteristic sizes ranging from the atomic scale to tens of nanometers such as C_{60} particles (Fig. 12).[168] This technique may allow identification of the nucleation position in the plasma reactor *in situ*.

Raman spectroscopy has been a powerful tool in the characterization of CNT and related carbon nanostructure growth. Carbon nanotube nucleation and growth can be detected by the appearance and increase in the G (graphite) and D (disordered) band peaks located at ~1590 and ~1350 cm^{-1}, respectively. In a recent CVD process, the intensity ratio between G and D band peaks (i.e., G/D ratio) and its time evolution were employed to monitor the growth rate of SWCNTs under different conditions *in situ*.[169] This allowed automation of the process optimization using an artificial intelligence (AI) planner and also mitigated reproducibility issues.[169] Similarly, the use of Raman spectroscopy inside a thermal plasma process could provide real time information of the growth kinetics of nanotubes. In this case, the spatial evolution of the G/D ratio along the reactor axis could be an excellent index for *in situ* monitoring of the growth rate of CNTs. However, combination of long measurement distance, fast growth speed, as well as plasma radiation represents a significant challenge. In addition, the vibration of nanotubes at high temperatures (>2000 K) is not well understood. It is also uncertain how resonance would be strong with the nanotubes freely suspended in the gas-phase. Lastly, this

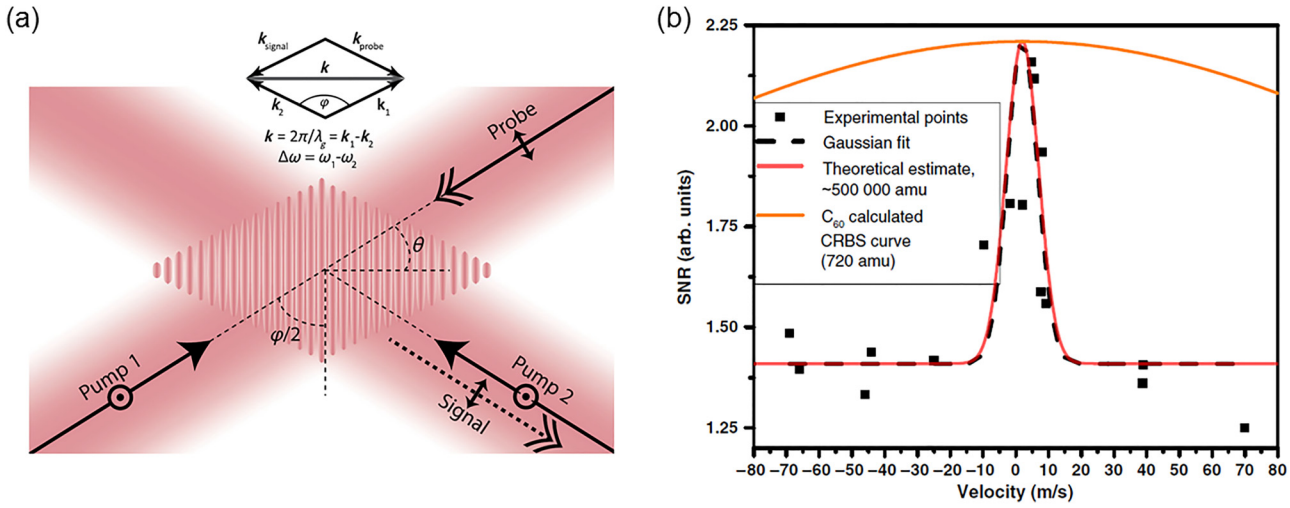

FIG. 12. Four-wave-mixing method for *in situ* volumetric detection of nanoparticles. (a) Schematic of the geometry of the planar coherent Rayleigh-Brillouin scattering (CRBS). (b) Reconstructed Rayleigh profile for nanoparticles from the ratio of the scattering-before-destruction CRBS signal. Reprinted with permission from Gerakis *et al.*, Phys. Rev. Appl. **9**, 014031 (2018). Copyright 2018 American Physical Society.

technique may not be applicable to monitoring BNNT growth because there is only one distinct Raman peak for hBN materials at ~1360 cm^{-1}, which is not specific to BNNTs or hBN particles.

Coagulation process is one of the main nanoparticle growth mechanisms and usually dictated by the Brownian-type coagulation, while it can be either improved or suppressed by the charging effect of nanoparticles in the plasma. Particles can be negatively charged by the free electrons in the plasma or can be positively charged by the electron emission mechanism such as thermionic emission, thus experiencing the Coulomb force from others (Fig. 13). Monitoring of the charge state of nanoparticles[170] is of critical importance to further control the particle size distribution or de-bundling of various 1D nanomaterials, which has been a critical issue in their practical applications. Several techniques, such as differential mobility analysis (DMA) as well as tandem differential mobility analysis (TDMA), have been utilized to analyze the charge state of nanoparticles during their synthesis by plasmas or flames.[170,171] However, little experimental study has been reported to understand charging dynamics of low-dimensional nanomaterials under plasma conditions. A theoretical study revealed that pristine CNTs and BNNTs have positive electron affinity, indicating that free electron transfer to the tube surfaces is always favorable for both nanotubes.[172] Hence, they are highly likely to be charged during the plasma process being bombarded by free electrons. The existence of stable nanotube anions may not only affect their aggregation or bundling process but also growth rates. A theory paper studied the adsorption and migration behavior of a carbon adatom on a negatively charged SWCNT and found that its migration distance toward metal catalyst significantly increases owing to the stronger bonding between the adsorbed carbon adatom and the carbon atoms of CNTs enhanced by the extra charges.[173]

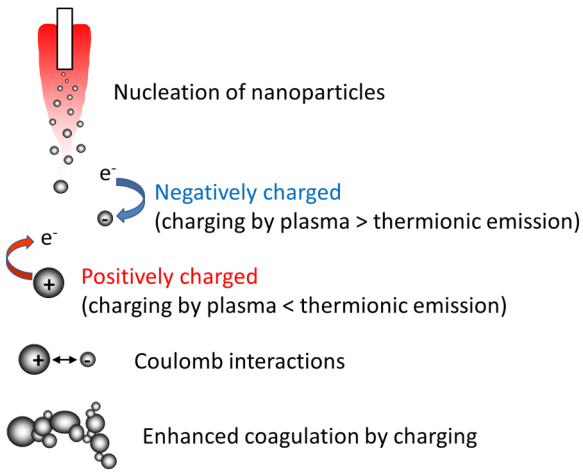

FIG. 13. Nanoparticle charging dynamics in the plasma jet and its effect on nanoparticle growth.

This resulted in a significant increment of carbon adatom flux toward the metal catalyst which may enhance the growth of SWCNTs.

C. Toward new revolutionary nanomaterials

1. Nanoscale high-entropy alloys

Multi-component nanoparticles consisting of five or more principle elements with an equimolar ratio demonstrated a wide range of interesting properties such as superconducting, supermagnetic, and plasmonic behaviors that are appealing for many applications. Despite their inherent tendency to segregate or order with similar elements, it has been demonstrated that such nanoparticles can be stabilized by their high configurational entropy in the liquid state and are named "high-entropy alloys" (HEAs).[174] However, upon their solidification, maintaining their uniform composition as a single nanoparticle (i.e., solid-state solution) is often highly challenging as the significance of the mixing entropy term in the free energy is reduced as the temperature decreases leading to phase-separation or internal ordering. This has greatly limited the composition space to not exceed three elements or to intermetallic nanoparticles with a defined stoichiometry and crystal structures. In the HEAs synthesis, the phase-separated thermodynamic equilibrium structure can be avoided by controlling the kinetics such as diffusion of species in a particle. For instance, rapid quenching can freeze the liquid alloy state to create solid-solution nanoparticles (Fig. 14).[175] Thermal plasma jets are capable of rapid heating of the feedstock to produce atomically mixed phases and also rapid cooling of those mixtures to form crystalline solid-solution nanoparticles.

2. Chirality-specific growth of SWCNTs

Electronic properties of SWCNTs largely depend on their chirality, thus requiring sorting of semiconducting and metallic nanotubes in advance to their specific applications. Since most synthesis methods produce nanotubes with mixed chiralities, the chirality-specific growth of SWCNTs is highly desirable to minimize nanotube separation efforts and often considered as the ultimate goal of SWCNT synthesis. The SWCNT nucleation is initiated by the formation of a sp^2-carbon cap on a catalyst nanoparticle and its structure usually dictates the structure of the nanotube grown (e.g., diameter, chirality). Thus, the efficient control of the cap structure would be the key to the chirality-specific growth of SWCNTs. For instance, the carbon cap can nucleate and grow epitaxially from the predefined faceted surface of a nanoparticle so that the chirality of a SWCNT can be determined [Fig. 15(a)]. Owing to the high carbon solubility, the melting point of transition metals widely used in the SWCNT synthesis usually drops substantially upon carbon dissolution by forming of a eutectic system. Therefore, these catalyst nanoparticles can be liquefied even at relatively low synthesis temperatures of 700–1100 °C, the surfaces being significantly reshaped or reconstructed during the SWCNT

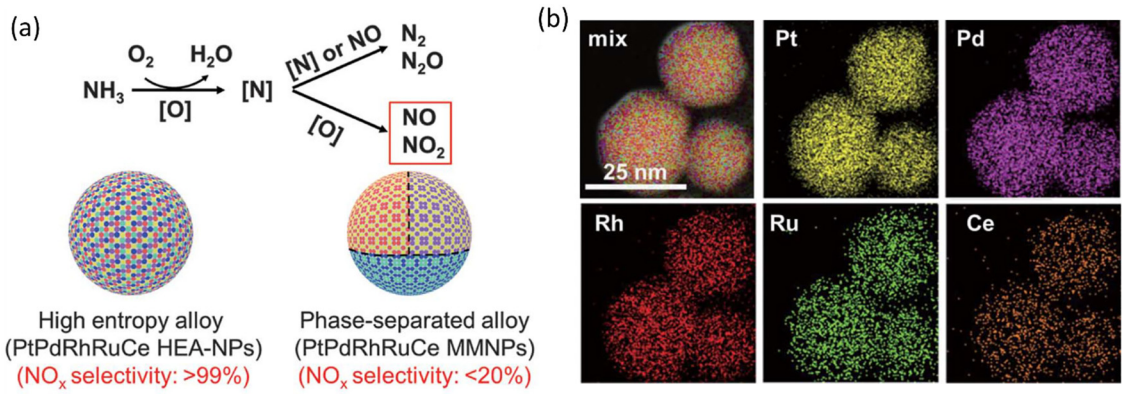

FIG. 14. Synthesis of high-entropy-alloy nanoparticles (HEA-NPs). (a) Schematic comparison of a phase-separated heterostructure and a high-entropy-alloy structure. (b) Quinary HEA-NPs (PtPdRhRuCe) synthesized by a carbothermal shock method. Reprinted with permission from Yao *et al.*, Science **359**, 1489 (2018). Copyright 2018 American Association for the Advancement of Science.

growth (i.e., vapor-liquid-solid growth mechanism).[176] This may cause the loss of control of the cap nucleation with a specific structure.[177] For this reason, researchers have started to explore high-melting point catalysts that can maintain their crystalline structures upon carbon adsorption without significant surface reconstruction [i.e., vapor-solid-solid growth mechanism, Fig. 15(a)]. A recent study showed that tungsten-based bimetallic alloys (e.g., W_6Co_7) were successful at growing SWCNTs with a single chirality of (12, 6).[178] Preparation of such high-melting point alloys is a challenging task requiring a high temperature environment and also a two-step process. The high temperature of the thermal plasma can be highly effective for *in situ* formation of such high-melting point nanoparticles with a high throughput, thus enabling the chirality-selective growth of SWCNT at large-scales in a single reactor.[179]

FIG. 15. Chirality-specific growth of SWCNTs. (a) Vapor-solid-solid (VSS) growth mechanism: a SWCNT grows by matching the crystal structure of a faceted metal nanoparticle thus the VSS growth mechanism has a good potential to control SWCNT diameter or chirality. (b) DFT simulation of templated growth of a SWCNT with a specific chirality (*n*, *m*) from a faceted W_6Co_7 intermetallic compound catalyst. Reprinted with permission from Li *et al.*, Top. Curr. Chem. **375**, 29 (2017). Copyright 2017 Springer International Publishing Switzerland.

3. In situ fabrication of hybrid nanomaterials

Decoration of low-dimensional nanomaterials with foreign metal or ceramic nanoparticles has great potential not only in improving the reactivity of nanomaterials toward other matrices but also providing additional set of functionality including new optical properties (e.g., localized surface plasma resonance) and catalytic activities. This is of particular interest in the nanotube science and technology as pristine CNTs or BNNTs are known to be chemically inert limiting their dispersion in various applications (Fig. 16).[180] At present, improvement of nanomaterial reactivity or functionality is mostly achieved by two-step procedures; nanomaterials are first synthesized and their surfaces are subsequently modified in a separate reactor through substitutional reactions (e.g., doping), physical vapor depositions, or complicated chemical functionalization.[180] The common drawback of this approach is that the entire process is time, energy, equipment, and chemically consuming.

In situ surface modification of nanomaterials by doping or decorating with foreign particles would be highly promising and an excellent alternative to the existing multi-step processes. The main advantage of this approach is that growth of nanomaterials and their subsequent surface modification take place simultaneously in just one reactor within a very short time period. However, such development has been very challenging because co-existence of foreign species usually interferes with nanomaterials formation, thus has detrimental effects on the nucleation and growth of nanomaterials with high quality and high purity. This makes it very difficult to achieve high loadings of foreign particles (e.g., 50 wt. %) with the existing *in situ* processes. Typically, the loading is around 5 wt. % or less.

For the successful *one-pot* synthesis of such hybrid nanomaterials, it would be crucial to separate the growth of two different materials to avoid interference with each other. The nanomaterial growth can precede the formation of foreign particles (i.e., dopants or decorating particles), resulting in nanomaterials being decorated by the foreign particles downstream. In this case, *delayed nucleation* of foreign particles would be key and can be achieved by the careful selection of foreign species based on their physico-chemical properties (e.g., melting temperature, saturation vapor pressure, solubility to seed nanomaterial) and precise control of the thermofluid fields (e.g., temperature and velocity gradients) along the

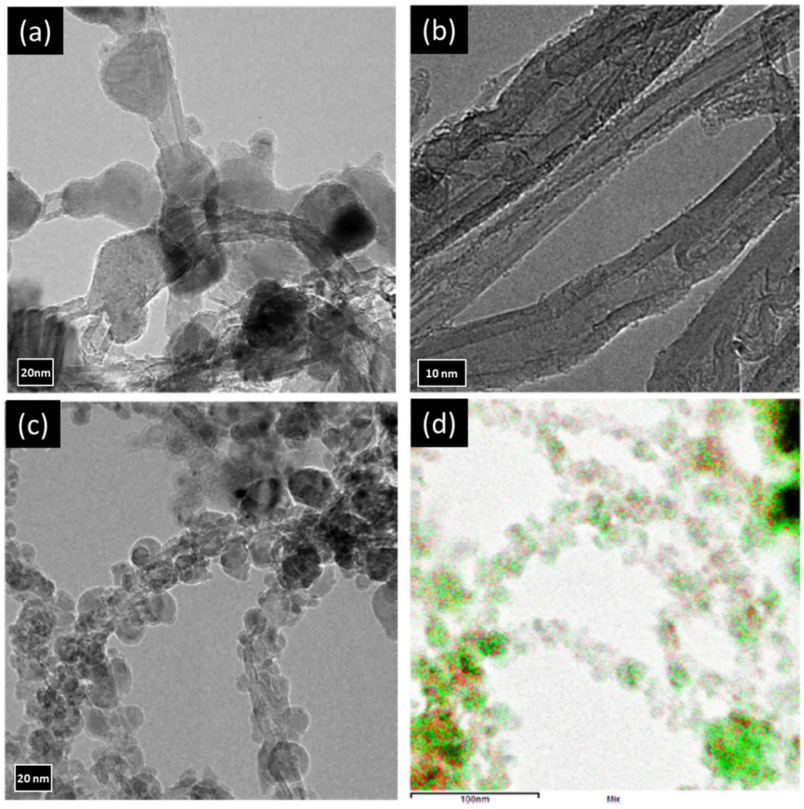

FIG. 16. TEM images of multi-walled carbon nanotubes (MWCNTs) decorated with silicon nanoparticles. (a) MWCNTs with silicon nanoparticles attached. (b) MWCNTs without silicon nanoparticles (c), (d) elemental map of the MWCNT/Si composite (red and green colors indicate carbon and silicon species, respectively). Reprinted with permission from Na *et al.*, Phys. Status Solidi **211**, 2749 (2014). Copyright 2014 John Wiley and Sons.

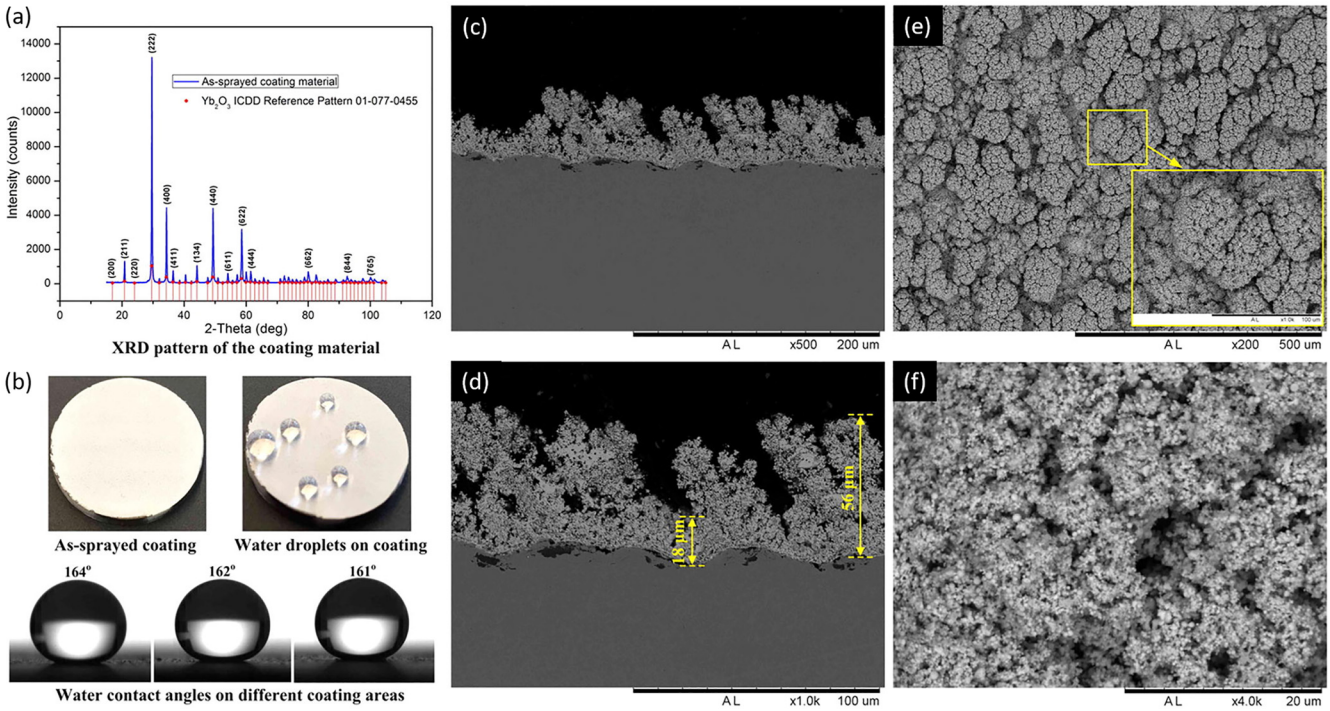

FIG. 17. Super-hydrophobic ceramic (Yb_2O_3) coating with a micro/nano hierarchical structure. The coating was prepared by an one-step, liquid precursor thermal plasma spray method. (a) X-ray diffraction pattern of the coating. (b) Super-hydrophobicity of the coating. (c)–(f) SEM images of the coating showing its micro/nano hierarchical structure. Reprinted with permission from Xu *et al*., Mater. Lett. **211**, 24 (2018). Copyright 2018 Elsevier B.V.

reactor axis. Thermal plasma jets are highly flexible with controlling their energy and flow, thus extremely well suited for the spatially distributed growth of multiple nanomaterials in a single reactor. This will allow cost-effective, *in situ* fabrication of various hybrid nanomaterials with customized reactivity and functionalities.

4. Coatings with micro/nano hierarchical structures

The surface properties can be modified by coatings with various functional materials. Although the resultant property of the surface is largely dictated by the property of the coated material, it is also determined by the detailed microstructure of the coating. Inspired from nature, thin films or coatings with micro/nano hierarchical structures (i.e., combination of nano and microstructures) have received much attention to provide surface texture-dependent properties such as super-hydrophobicity, optical transparency, and antireflection. Thermal plasma jets are capable of fabricating nanoparticles and also making their durable coating on various surfaces *in situ*. The microstructure of the coating is commonly controlled by tailoring the plasma spaying parameters which is highly attractive for the one-step fabrication of a coating with a hierarchical structure. For instance, such structures can be formed by plasma spraying of liquid feedstock or injection of agglomerated nanoparticles.[181,182] Recently, super-hydrophobic ceramic (Yb_2O_3) coatings were successfully fabricated using solution precursor plasma spray (DC 40 kW, 101 kPa, Ar/H_2 plasma).[183] The coatings had an array of micron-size, cauliflower-like clusters composed of agglomerated Yb_2O_3 nanoparticles which were produced from the direct decomposition of a liquid precursor of $Yb(NO_3)_3{\cdot}H_2O$ in the DC plasma jet (Fig. 17). Thanks to this two-length scale hierarchical structure, the coating exhibited super-hydrophobicity with a contact angle over 150° and a water roll-off angle about 6.5°. To get better control of the microstructure, optimization of the aerodynamics of the nanoparticles produced would be one of the main interests in this emerging area.

ACKNOWLEDGMENTS

The authors acknowledge support from the National Research Council of Canada's (NRC) Security Materials Technology Program and National Research Foundation of Republic of Korea (No. NRF-2010 0020077) and thank Robyn Iannitto at McGill University for her proofreading of this paper. This work was supported by the Technology Innovation Program (2000479) funded By the Ministry of Trade, Industry & Energy (MOTIE, Korea).

REFERENCES

[1]M. I. Boulos, P. Fauchais, and E. Pfender, *Thermal Plasmas: Fundamentals and Applications* (Plenum Press, New York, 1994), Vol. 1.
[2]M. I. Boulos, IEEE Trans. Plasma Sci. **19**, 1078 (1991).
[3]P. Fauchais and A. Vardelle, IEEE Trans. Plasma Sci. **25**, 1286 (1997).
[4]E. Pfender, Plasma Chem. Plasma Process. **19**, 1 (1999).
[5]A. B. Murphy and D. Uhrlandt, Plasma Sources Sci. Technol. **27**, 063001 (2018).
[6]I. M. MacKinnon and B. G. Reuben, J. Electrochem. Soc. **122**, 806 (1975).
[7]S. M. L. Hamblyn and B. G. Reuben, Adv. Inorg. Chem. Radiochem. **17**, 89 (1975).
[8]T. Yoshida, A. Kawasaki, K. Nakagawa, and K. Akashi, J. Mater. Sci. **14**, 1624 (1979).
[9]P. C. Kong and Y. C. Lau, Pure Appl. Chem. **62**, 1809 (1990).
[10]P. Fauchais, A. Vardelle, and A. Denoirjean, Surf. Coat. Technol. **97**, 66 (1997).
[11]D. Vollath, J. Nanopart. Res. **10**, 39 (2008).
[12]M. Shigeta and A. B. Murphy, J. Phys. D Appl. Phys. **44**, 174025 (2011).
[13]J.-H. Seo and B.-G. Hong, Nucl. Eng. Technol. **44**, 9 (2012).
[14]H. W. Kroto, J. R. Heath, S. C. O'Brien, R. F. Curl, and R. E. Smalley, Nature **318**, 162 (1985).
[15]S. Iijima, Nature **354**, 56 (1991).
[16]K. S. Novoselov, A. K. Geim, S. V. Morozov, D. Jiang, Y. Zhang, S. V. Dubonos, I. V. Grigorieva, and A. A. Firsov, Science **306**, 666 (2004).
[17]J. Peters, F. Yin, C. F. M. Borges, J. Heberlein, and C. Hackett, J. Phys. D Appl. Phys. **33**, 1781 (2005).
[18]L. Pershin, A. Mitrasinovic, and J. Mostaghimi, J. Phys. D Appl. Phys. **46**, 224019 (2013).
[19]M. Hur, K. S. Kim, and S. H. Hong, Plasma Sources Sci. Technol. **12**, 255 (2003).
[20]J. R. Fincke, W. D. Swank, S. C. Snyder, and D. C. Haggard, Rev. Sci. Instrum. **64**, 3585 (1993).
[21]M. Rahmane, G. Soucy, and M. I. Boulos, Rev. Sci. Instrum. **66**, 3424 (1995).
[22]S. Choi, T. H. Hwang, J. H. Seo, D. U. Kim, and S. H. Hong, IEEE Trans. Plasma Sci. **32**, 473 (2004).
[23]M. Shigeta, J. Phys. D Appl. Phys. **49**, 493001 (2016).
[24]M. I. Boulos, Pure Appl. Chem. **57**, 1321 (1985).
[25]J. Guo, *Induction Plasma Synthesis of Nanomaterials* (IntechOpen, 2016).
[26]M. Moisan and Z. J. Zakrzewski, J. Phys. D Appl. Phys. **24**, 1025 (1991).
[27]H. S. Uhm, Y. C. Hong, and D. H. Shin, Plasma Sources Sci. Technol. **15**, S26 (2006).
[28]D. Szabó and S. Schlabach, Inorganics **2**, 468 (2014).
[29]S. H. Lee, S. M. Oh, and D. W. Park, Mater. Sci. Eng. C **27**, 1286 (2007).
[30]A. B. Murphy, J. Phys. D Appl. Phys. **37**, 2841 (2004).
[31]I. Bica, J. Magn. Magn. Mater. **201**, 45 (1999).
[32]K. Suresh, V. Selvarajan, and I. Mohai, Vacuum **82**, 482 (2008).
[33]S. J. Lee, T. H. Kim, D. W. Kim, and D. W. Park, Plasma Chem. Plasma Process. **37**, 967 (2017).
[34]S. Choi, H. Lee, and D. W. Park, J. Nanomater. **2016**, 5849041 (2016).
[35]V. Colombo, E. Ghedini, M. Gherardi, and P. Sanibondi, Plasma Sources Sci. Technol. **21**, 55007 (2012).
[36]J. Guo, X. Fan, R. Dolbec, S. Xue, J. Jurewicz, and M. Boulos, Plasma Sci. Technol. **12**, 188 (2010).
[37]Y.-L. Li and T. Ishigaki, J. Phys. Chem. B **108**, 15536 (2004).
[38]Kim, H. G. Jeong, and D. Park, Sci. Adv. Mater. **9**, 1637 (2017).
[39]J.-G. Li, M. Ikeda, R. Ye, Y. Moriyoshi, and T. Ishigaki, J. Phys. D Appl. Phys. **40**, 2348 (2007).
[40]C. Y. Tsai, H. C. Hsi, T. H. Kuo, Y. M. Chang, and J. H. Liou, Aerosol Air Qual. Res. **13**, 639 (2013).
[41]J. W. Park, D. W. Kim, H. S. Seon, K. S. Kim, and D. W. Park, Thin Solid Films **518**, 4113 (2010).
[42]J. E. Lee, S. M. Oh, and D. W. Park, Thin Solid Films **457**, 230 (2004).
[43]C. Y. Tsai, H. C. Hsi, H. Bai, K. S. Fan, and H. D. Sun, Jpn. J. Appl. Phys. **51**, 01AL01 (2012).
[44]S.-M. Oh, M. Cappelli, and D.-W. Park, Korean J. Chem. Eng. **19**, 903 (2002).
[45]L. Tong and R. G. Reddy, Scr. Mater. **52**, 1253 (2005).
[46]T. Ishigaki, S. M. Oh, J. G. Li, and D. W. Park, Sci. Technol. Adv. Mater. **6**, 111 (2005).
[47]P. Ronsheim, L. E. Toth, A. Mazza, E. Pfender, and B. Mitrofanov, J. Mater. Sci. **16**, 2665 (1981).
[48]T. Ryu, H. Y. Sohn, K. S. Hwang, and Z. Z. Fang, J. Am. Ceram. Soc. **92**, 655 (2009).
[49]A. V. Samokhin, N. V. Alekseev, S. A. Kornev, M. A. Sinaiskii, Y. V. Blagoveschenskiy, and A. V. Kolesnikov, Plasma Chem. Plasma Process. **33**, 605 (2013).
[50]P. V. Krasovskii, O. S. Malinovskaya, A. V. Samokhin, Y. V. Blagoveshchenskiy, V. A. Kazakov, and A. A. Ashmarin, Appl. Surf. Sci. **339**, 46 (2015).
[51]T. Ryu, H. Y. Sohn, K. S. Hwang, and Z. Z. Fang, J. Mater. Sci. **43**, 5185 (2008).
[52]Y. Tian, Y. Jia, Y. Bao, and Y. Chen, Diam. Relat. Mater. **16**, 302 (2007).
[53]S.-M. Oh and D.-W. Park, Thin Solid Films **316**, 189 (1998).
[54]T.-H. Kim, S. Choi, and D.-W. Park, J. Korean Phys. Soc. **63**, 1864 (2013).
[55]Y. Chang, R. M. Young, and E. Pfender, Plasma Chem. Plasma Process. **7**, 299 (1987).
[56]S. D. F. Allarie, J. Mater. Sci. **26**(**26**), 6736 (1991).
[57]G. Hou, B. Cheng, F. Ding, M. Yao, P. Hu, and F. Yuan, ACS Appl. Mater. Interfaces **7**, 2873 (2015).
[58]C. U. Bang, Y. C. Hong, and H. S. Uhm, Surf. Coat. Technol. **201**, 5007 (2007).
[59]A. V. Samokhin, V. A. Sinaiskii, N. V. Alekseev, E. V. Troitskaya, and Y. V. Tsvetkov, Inorg. Mater. Appl. Res. **5**, 224 (2014).
[60]M. Kakati, B. Bora, S. Sarma, B. J. Saikia, T. Shripathi, U. Deshpande, A. Dubey, G. Ghosh, and A. K. Das, Vacuum **82**, 833 (2008).
[61]D. W. Kim, T. H. Kim, H. W. Park, and D. W. Park, Appl. Surf. Sci. **257**, 5375 (2011).
[62]E. H. Ko, T.-H. Kim, S. Choi, and D.-W. Park, J. Nanosci. Nanotechnol. **15**, 8515 (2015).
[63]T. Kim, E. H. Ko, J. Nam, S. E. Shim, and D. Park, J. Nanosci. Nanotechnol. **17**, 9217 (2017).
[64]T. Watanabe, A. Nezu, Y. Abe, Y. Ishii, and K. Adachi, Thin Solid Films **435**, 27 (2003).
[65]T.-H. Kim, S. Choi, and D.-W. Park, Nanomaterials **6**, 38 (2016).
[66]S. Choi, J. Matsuo, and T. Watanabe, J. Phys. Conf. Ser. **441**, 12030 (2013).
[67]Y. Cheng, M. Shigeta, S. Choi, and T. Watanabe, Chem. Eng. J. **183**, 483 (2012).
[68]Y. Cheng, S. Choi, and T. Watanabe, Powder Technol. **246**, 210 (2013).
[69]S. Choi, L. D. S. Lapitan, Y. Cheng, and T. Watanabe, Adv. Powder Technol. **25**, 365 (2014).
[70]Y. Cheng, S. Choi, and T. Watanabe, J. Phys. Conf. Ser. **441**, 12031 (2013).
[71]Y. Cheng, M. Tanaka, T. Watanabe, S. Y. Choi, M. S. Shin, and K. H. Lee, J. Phys. Conf. Ser. **518**, 12026 (2014).
[72]S. T. Park, T. H. Kim, and D. W. Park, Appl. Surf. Sci. **374**, 257 (2016).
[73]M. Tanaka, J. Noda, T. Watanabe, J. Matsuno, and A. Tsuchiyama, J. Phys. Conf. Ser. **518**, 12025 (2014).
[74]T. H. Kim, A. Tsuchiyama, A. Takigawa, and J. Matsuno, in *Proceedings of the 23rd International Symposium on Plasma Chemistry, Montreal, Canada, 30 July–4 August 2017* (Internal Plasma Chemistry Society, 2017).
[75]K. T. Keitaro Nakamura, A. Kinoshita, S. Watanabe, and N. Uemura, J. Soc. Powder Technol. Jpn. **50**, 495 (2013).
[76]S. Choi, M. S. Lee, and D. W. Park, Curr. Appl. Phys. **14**, 433 (2014).
[77]M. Shin, K. Lee, J. Kim, S. Choi, G. Cho, and S. Kim, J. Nanosci. Nanotechnol. **15**, 9045 (2015).
[78]Y. S. Na, H. Yoo, T. H. Kim, J. Choi, W. I. Lee, S. Choi, and D. W. Park, Thin Solid Films **587**, 14 (2015).
[79]K. P. Shinde, M. Ranot, C. J. Choi, H. S. Kim, and K. C. Chung, AIP Adv. **7**, 75013 (2017).
[80]J. Borysiuk, A. Grabias, J. Szczytko, M. Bystrzejewski, A. Twardowski, and H. Lange, Carbon **46**, 1693 (2008).
[81]M. Bystrzejewski, S. Cudziło, A. Huczko, H. Lange, G. Soucy, G. Cota-Sanchez, and W. Kaszuwara, Biomol. Eng. **24**, 555 (2007).

[82]A. K. Geim and P. Kim, Sci. Am. **298**, 90 (2008).
[83]R. E. Smalley and B. I. Yakobson, Solid State Commun. **107**, 597 (1998).
[84]W. Kratschmer, L. D. Lamb, K. Fostiropoulos, and D. R. Huffman, Nature **347**, 354 (1990).
[85]C. Wang, T. Imahori, Y. Tanaka, T. Sakuta, H. Takikawa, and H. Matsuo, Thin Solid Films **390**, 31 (2001).
[86]G. Cota-Sanchez, G. Soucy, A. Huczko, and H. Lange, Carbon **43**, 3153 (2005).
[87]B. Todorovic-Markovic, Z. Markovic, I. Mohai, Z. Karoly, L. Gai, K. Foglein, P. T. Szabo, and J. Szepvolgyi, Chem. Phys. Lett. **378**, 434 (2003).
[88]J. Szepvolgyi, Z. Markovic, B. Todorovic-Markovic, Z. Nikolic, I. Mohai, Z. Farkas, M. Toth, E. Kovats, P. Scheier, and S. Feil, Plasma Chem. Plasma Process. **26**, 597 (2006).
[89]K. Yoshie, S. Kasuya, K. Eguchi, and T. Yoshida, Appl. Phys. Lett. **61**, 2782 (1992).
[90]R. Saito, G. Dresselhaus, and M. S. Dresselhaus, *Physical Properties of Carbon Nanotubes* (World Scientific, 1998).
[91]R. H. Baughman, A. A. Zakhidov, and W. A. de Heer, Science **297**, 787 (2002).
[92]M. F. L. De Volder, S. H. Tawfick, R. H. Baughman, and A. J. Hart, Science **339**, 535 (2013).
[93]O. Smiljanic, B. L. Stansfield, J. P. Dodelet, A. Serventi, and S. Desilets, Chem. Phys. Lett. **356**, 189 (2002).
[94]S. I. Choi, J. S. Nam, J. I. Kim, T. H. Hwang, J. H. Seo, and S. H. Hong, Thin Solid Films **506**, 244 (2006).
[95]S. I. Choi, J. S. Nam, C. M. Lee, S. S. Choi, J. I. Kim, J. M. Park, and S. H. Hong, Curr. Appl. Phys. **6**, 224 (2006).
[96]J. Hahn, J. H. Han, J.-E. Yoo, H. Y. Jung, and J. S. Suh, Carbon **42**, 877 (2004).
[97]J. Hahn, H. Y. Jung, D. W. Kang, J.-E. Yoo, and J. S. Suh, Carbon **42**, 3024 (2004).
[98]J. Hahn, S. B. Heo, and J. S. Suh, Carbon **43**, 2638 (2005).
[99]K. S. Kim, G. Cota-Sanchez, C. T. Kingston, M. Imris, B. Simard, and G. Soucy, J. Phys. D Appl. Phys. **40**, 2375 (2007).
[100]K. S. Kim, M. Imris, A. Shahverdi, Y. Alinejad, and G. Soucy, J. Phys. Chem. C **113**, 4340 (2009).
[101]K. S. Kim, C. T. Kingston, D. Ruth, M. Barnes, and B. Simard, Chem. Eng. J. **250**, 331 (2014).
[102]K. S. Novoselov, A. K. Geim, S. V. Morozov, D. Jiang, M. I. Katsnelson, I. V. Grigorieva, S. V. Dubonos, and A. A. Firsov, Nature **438**, 197 (2005).
[103]A. K. Geim, Science **324**, 1530 (2009).
[104]K. S. Kim, S. H. Hong, K. Lee, and W. T. Ju, IEEE Trans. Plasma Sci. **35**, 434 (2007).
[105]K. S. Kim, J. H. Seo, J. S. Nam, W. T. Ju, and S. H. Hong, IEEE Trans. Plasma Sci. **33**, 813 (2005).
[106]J. Kim, S. B. Heo, G. H. Gu, and J. S. Suh, Nanotechnology **21**, 095601 (2010).
[107]R. Pristavita, N.-Y. Mendoza-Gonzalez, J.-L. Meunier, and D. Berk, Plasma Chem. Plasma Process. **30**, 267 (2010).
[108]R. Pristavita, J.-L. Meunier, and D. Berk, Plasma Chem. Plasma Process. **31**, 393 (2011).
[109]J.-L. Meunier, N.-Y. Mendoza-Gonzalez, R. Pristavita, D. Binny, and D. Berk, Plasma Chem. Plasma Process. **34**, 505 (2014).
[110]H. Zhang, T. Cao, and Y. Cheng, Carbon **86**, 38 (2015).
[111]S. Y. Choi, M. Mamak, E. Cordola, and U. Stadler, J. Mater. Chem. **21**, 5142 (2011).
[112]L. A. Ponomarenko, F. Schedin, M. I. Katsnelson, R. Yang, E. W. Hill, K. S. Novoselov, and A. K. Geim, Science **320**, 356 (2008).
[113]J. Kim and J. S. Suh, ACS Nano **8**, 4190 (2014).
[114]R. Arenal, X. Blase, and A. Loiseau, Adv. Phys. **59**, 101 (2010).
[115]C. Y. Zhi, Y. Bando, C. C. Tang, and D. Golberg, Mater. Sci. Eng. Res. **70**, 92 (2010).
[116]D. Golberg, Y. Bando, Y. Huang, T. Terao, M. Mitome, C. Tang, and C. Zhi, ACS Nano **4**, 2979 (2010).
[117]A. Rubio, J. L. Corkill, and M. L. Cohen, Phys. Rev. B **49**, 5081 (1994).
[118]K. S. Kim, M. B. Jakubinek, Y. Martinez-Rubi, B. Ashrafi, J. Guan, K. O'Neill, M. Plunkett, A. Hrdina, S. Lin, S. Denommee, C. T. Kingston, and B. Simard, RSC Adv. **5**, 41186 (2015).
[119]N. G. Chopra, R. J. Luyken, K. Cherrey, V. H. Crepsi, M. L. Cohen, S. G. Louie, and A. Zettl, Science **269**, 966 (1995).
[120]K. S. Kim, M. J. Kim, C. Park, C. C. Fay, S.-H. Chu, C. T. Kingston, and B. Simard, Semicond. Sci. Technol. **32**, 013003 (2017).
[121]R. Arenal, O. Stephan, J. L. Cochon, and A. Loiseau, J. Am. Chem. Soc. **129**, 16183 (2007).
[122]C. S. Yoo, J. Akella, H. Cynn, and M. Nicol, Phys. Rev. B **56**, 140 (1997).
[123]M. W. Smith, K. C. Jordan, C. Park, J.-W. Kim, P. T. Lillehei, R. Crooks, and J. Harrison, Nanotechnology **20**, 505604 (2009).
[124]K. S. Kim, C. T. Kingston, A. Hrdina, M. B. Jakubinek, J. Guan, M. Plunkett, and B. Simard, ACS Nano **8**, 6211 (2014).
[125]K. S. Kim, M. Couillard, H. Shin, M. Plunkett, D. Ruth, C. T. Kingston, and B. Simard, ACS Nano **12**, 884 (2018).
[126]P. S. Krstic, L. Han, S. Irle, and H. Nakai, Chem. Sci. **9**, 3803 (2018).
[127]A. Fathalizadeh, T. Pham, W. Mickelson, and A. Zettl, Nano Lett. **14**, 4881 (2014).
[128]J. Cumings and A. Zettl, Chem. Phys. Lett. **316**, 211 (2000).
[129]S. Bernard, V. Salles, J. Li, A. Brioude, M. Bechelany, U. B. Demircia, and P. Miele, J. Mater. Chem. **21**, 8694 (2011).
[130]R. Tenne, Nat. Nanotechnol. **1**, 103 (2006).
[131]Z. J. Han, A. T. Murdock, D. H. Seo, and A. Bendavid, 2D Mater. **5**, 032002 (2018).
[132]S.-C. Liao, H.-F. Lin, S.-W. Hung, and C.-T. Hu, J. Vac. Sci. Technol. B **24**, 1322 (2006).
[133]C. Balasubramanian, V. P. Godbole, V. K. Rohatgi, A. K. Das, and S. V. Bhoraskar, Nanotechnology **15**, 370 (2004).
[134]Y. Ishisaka, N. Kodama, Y. Tanaka, Y. Uesugi, T. Ishijima, S. Sueyasu, S. Watanabe, and K. Nakamura, Appl. Phys. Express **10**, 096201 (2017).
[135]M. I. Boulos, Plasma Chem. Plasma Process. **36**, 3 (2016).
[136]A. Gleizes, J. J. Gonzalez, and P. Freton, J. Phys. D Appl. Phys. **38**, R153 (2005).
[137]P. Proulx and J.-F. Bilodeau, Plasma Chem. Plasma Process. **11**, 371 (1991).
[138]A. C. D. Cruz and R. J. Munz, IEEE Trans. Plasma Sci. **25**, 1008 (1997).
[139]N. Y. Mendoza-Gonzalez, B. M. Goortani, and P. Proulx, Mater. Sci. Eng. C **27**, 1265 (2007).
[140]M. Shigeta and T. Watanabe, J. Phys. D Appl. Phys. **40**, 2407 (2007).
[141]K. S. Kim, A. Moradian, J. Mostaghimi, Y. Alinejad, A. Shahverdi, B. Simard, and G. Soucy, Nano Res. **2**, 800 (2009).
[142]C. T. Crowe, M. P. Sharma, and D. E. Stock, J. Fluids Eng. **99**, 325 (1977).
[143]S. L. Girshick, P. C. Chiu, and P. H. McMurry, Aerosol Sci. Technol. **13**, 465 (1990).
[144]S. L. Girshick, Plasma Sources Sci. Technol. **3**, 388 (1994).
[145]P. J. Bruggeman *et al.*, Plasma Sources Sci. Technol. **25**, 053002 (2016).
[146]M. Shigeta and T. Watanabe, J. Therm. Spray Technol. **18**, 1022 (2009).
[147]M. Shigeta and T. Watanabe, J. Appl. Phys. **108**, 043306 (2010).
[148]J. A. Elliott, Y. Shibuta, H. Amara, C. Bichard, and E. C. Neyts, Nanoscale **5**, 6662 (2013).
[149]S. K. Friedlander, *Smoke, Dust and Haze: Fundamentals of Aerosol Dynamics*, 2nd ed. (Oxford University Press, Oxford, 2000).
[150]S. Tashiro, T. Zeniya, K. Yamamoto, M. Tanaka, K. Nakata, A. B. Murphy, E. Yamamoto, K. Yamazaki, and K. Suzuki, J. Phys. D Appl. Phys. **43**, 434012 (2010).
[151]M. Boselli, V. Colombo, E. Ghedini, M. Gherardi, and P. Sanibondi, J. Phys. D Appl. Phys. **46**, 224006 (2013).
[152]M. Shigeta, S. Minami, and M. Tanaka, Weld. World **62**, 203 (2018).
[153]M. Li, X. Liu, X. Zhao, F. Yang, X. Wang, and Y. Li, Top. Curr. Chem. **375**, 29 (2017).
[154]J. Pousse, B. Chervy, J. F. Bilodeau, and A. Gleizes, Plasma Chem. Plasma Process. **16**, 605 (1996).
[155]W. Wang, M. Rong, A. B. Murphy, Y. Wu, J. W. Spencer, J. D. Yan, and M. T. C. Fang, J. Phys. D Appl. Phys. **44**, 355207 (2011).
[156]M. Schnick, U. Füssel, M. Hertel, A. Spille-Kohoff, and A. B. Murphy, J. Phys. D Appl. Phys. **43**, 022001 (2010).

[157]P. Gnoffo and C. C. Fay, J. Thermophys. Heat Transfer **27**, 369 (2013).
[158]T. Thajudeen, R. Gopalakrishnan, and C. J. Hogan, Aerosol Sci. Technol. **46**, 1174 (2012).
[159]S. Tashiro, A. B. Murphy, S. Matsui, and M. Tanaka, J. Phys. D Appl. Phys. **46**, 224007 (2013).
[160]Y. Tanaka, J. Phys. D Appl. Phys. **37**, 1190 (2004).
[161]S. A. Esfarjani, S. B. Dworkin, J. Mostaghimi, K. S. Kim, C. T. Kingston, B. Simard, and G. Soucy, J. Phys. Conf. Ser. **406**, 012011 (2012).
[162]A. Khrabry *et al.*, e-print arXiv:1810.09586 (2018).
[163]S. Hofmann *et al.*, Nano Lett. **7**, 602 (2007).
[164]E. Pigos, E. S. Penev, M. A. Ribas, R. Sharma, B. I. Yakobson, and A. R. Harutyunyan, ACS Nano **5**, 10096 (2011).
[165]P. Fauchais, J. F. Coudert, and M. Vardelle, "Diagnostics in thermal plasma," in *Plasma Diagnostics* (Academic, Boston, MA, 1989), p. 349.
[166]C. Stratton, A. Gerakis, I. Kaganovich, M. Keidar, A. Khrabry, J. Mitrani, Y. Raitses, M. N. Shneider, V. Vekselman, and S. Yatom, Plasma Sources Sci. Technol. **27**, 084001 (2018).
[167]S. Yatom, J. Bak, A. Khrabryi, and Y. Raitses, Carbon **117**, 154 (2017).
[168]A. Gerakis, Y.-W. Yeh, M. N. Shneider, J. M. Mitrani, B. C. Stratton, and Y. Raitses, Phys. Rev. Appl. **9**, 014031 (2018).
[169]P. Nikolaev *et al.*, npj Comput. Mater. **2**, 16031 (2016).
[170]X. Wang, J. Hafiz, R. Mukherjee, T. Renault, J. Heberlein, S. L. Girshick, and P. H. McMurry, Plasma Chem. Plasma Process. **25**, 439 (2005).
[171]S. H. Kim, K. S. Woo, B. Y. H. Liu, and M. R. Zachariah, J. Colloid Interface Sci. **282**, 46 (2005).
[172]H. Shin, J. Guan, M. Z. Zgierski, K. S. Kim, C. T. Kingston, and B. Simard, ACS Nano **9**, 12573 (2015).
[173]L. Han, P. Krstic, I. Kaganovich, and R. Car, Carbon **116**, 174 (2017).
[174]J.-W. Yeh, S.-K. Chen, S.-J. Lin, J.-Y. Gan, T.-S. Chin, T.-T. Shun, C.-H. Tsau, and S.-Y. Chang, Adv. Eng. Mater. **6**, 299 (2004).
[175]Y. Yao *et al.*, Science **359**, 1489 (2018).
[176]A. Harutyunyan, T. Tokune, and E. Mora, Appl. Phys. Lett. **87**, 051919 (2005).
[177]Z. Xu, T. Yan, and F. Ding, Chem. Sci. **6**, 4704 (2015).
[178]F. Yang *et al.*, Nature **510**, 522 (2014).
[179]H. Na, W. Lee, and H. Choi, Int. J. Refract. Met. Hard Mater. **53**, 17 (2015).
[180]Y.-S. Na, S. Choi, and D.-W. Park, Phys. Status Solidi **211**, 2749 (2014).
[181]K. VanEvery *et al.*, J. Therm. Spray Technol. **20**, 817 (2011).
[182]R. S. Lima and B. R. Marple, J. Therm. Spray Technol. **16**, 40 (2007).
[183]P. Xu, L. Pershin, J. Mostaghimi, and T. W. Coyle, Mater. Lett. **211**, 24 (2018).